

Deep generative modeling for financial time series with application in VaR: a comparative review *

Lars Ericson, Xuejun Zhu, Xusi Han, Rao Fu,

Shuang Li, Steve Guo, Ping Hu

This Version: January 18, 2024

Abstract

In the financial services industry, forecasting the risk factor distribution conditional on the history and the current market environment is the key to market risk modeling in general and value at risk (VaR) model in particular. As one of the most widely adopted VaR models in commercial banks, Historical simulation (HS) uses the empirical distribution of daily returns in a historical window as the forecast distribution of risk factor returns in the next day. The objectives for financial time series generation are to generate synthetic data paths with good variety, and similar distribution and dynamics to the original historical data. In this paper, we apply multiple existing deep generative methods (e.g., CGAN, CWGAN, Diffusion, and Signature WGAN) for conditional time series generation, propose and test two new methods for conditional multi-step time series generation, namely Encoder-Decoder CGAN and Conditional TimeVAE. Furthermore, we introduce a comprehensive framework with a set of KPIs to measure the quality of the generated time series for financial modeling. The KPIs cover distribution distance, autocorrelation and back-testing. All models (HS, parametric and neural networks) are tested on both historical USD yield curve data and additional data simulated from GARCH and CIR processes. The study shows that top performing models are HS, GARCH and CWGAN models. Future research directions in this area are also discussed.

Key words: distribution, GAN, conditional GAN, Wasserstein distance, diffusion, signature, historical simulation, GARCH, Vasicek, volatility clustering.

Journal-classification: C15, C32, C45, C53

*Corresponding author: Steve Guo (steve.guo@wellsfargo.com). All authors are with Wells Fargo. Email addresses are at the end of the paper. We thank the following for providing helpful comments on earlier drafts, Paul Romanelli and Jeffrey Kung.

©2024 Wells Fargo Bank, N. A. All rights reserved. The views expressed in this publication are our personal views and do not necessarily reflect the views of Wells Fargo Bank, N.A., its parent company, affiliates and subsidiaries.

1 Introduction

In financial risk management and analytics, it is a matter of great importance to forecast the future ¹. For example, forecasting the timing and direction of stock market moves is important for investment decisions. Forecasting the correlation of returns is important for asset allocation decisions (in the context of the Markowitz mean-variance framework). And forecasting the distribution of profit and loss (P&L) of a portfolio is important for market and counterparty risk management and regulatory capital calculation using Value at Risk (VaR) and even Expected Shortfall measures. VaR is a quantile of the portfolio P&L distribution in a future period. P&L distribution is calculated from the risk factor (return) distribution for a given portfolio using valuation models. Forecasting the risk factor distribution conditional on the history and the current market environment is the key to a good VaR model. One of the most widely used VaR models at commercial banks adopts historical simulation (HS) (Perignon and Smith (2010)), which uses the empirical distribution of daily returns in a historical window as the forecast distribution of risk factor returns in the next day. See Barone-Adesi et al. (1999) and BARONE-ADESI and GIANNOPOULOS (2001) for descriptions of historical simulation and the improved filtered historical simulation (FHS). However, the HS method is based on limited historical scenarios and may not provide an accurate description of the tails of the distributions for VaR calculation.

Generative Artificial Intelligence (or Generative AI) refers to deep-learning models that can generate high-quality text, images, and other content based on the data they were trained on ². Generative AI has the potential to bring breakthrough changes to many industries. Recently, an AI chatbot, ChatGPT, a generative large language model (LLM) introduced by OpenAI, is redefining the business of online searching and content creation. In image processing, Generative Adversarial Networks (GANs) have been a success to generate real-like images and enhance image resolutions. After image and text applications were developed, GANs were expanded to financial time series generation Fu et al. (2019), which allows us to enrich the available data for model development and testing. These upsides have led to a high level of investment in GAN technology in 2022 and 2023 ³. These are some of the institutions that have publicized GAN applications, for example, Fujitsu generates applicant-friendly loan denial explanations (Ramya Malur Srinivasan (2020)). UBS uses synthetic data to enable usage or sharing of information while protecting real data, to address gaps and weaknesses of real data, to create data around rare events from crises to fraud that is scarce by nature, to overcome training data shortages (Johnson (2020)). Interestingly, there is a legal case involving creation and use of synthetic customer data ⁴. JP Morgan has been engaging in high profile

¹Given that the financial markets are efficient generally, forecast in this context means a distribution forecast rather than a point forecast.

²<https://research.ibm.com/blog/what-is-generative-ai>

³<https://www.nytimes.com/2023/01/07/technology/generative-ai-chatgpt-investments.html>.

⁴See “Fake Accounts And Fake Data: The Good, The Bad And The Preventable”

research and methodology development of deep hedging⁵. Deep hedging is outside the scope of this study.

The objectives for financial time series generation are to generate synthetic data that look real and with good variability. If the synthetic data are too different from real data, models that are trained on synthetic data may not be generalizable to real data. However, if the synthetic data are too close to real data (e.g. having a very high correlation), then they may not be useful complements to real data. Furthermore, for VaR and market risk modeling, the key focus is to forecast the conditional distribution of P&L for a specific future horizon, given the history and recent market conditions. In this paper, we apply multiple existing deep learning methods for conditional multi-step time series generation, and they are described in Section 2. We propose and test two new deep learning methods for conditional multi-step time series generation in Section 2, which are Encoder-Decoder CGAN (Fu (2022)) and Conditional TimeVAE (VAE for short). We test these methods on both simulated data (Sections 3 and 4.4) and real USD yield curves (Section 4.5).

Furthermore, we introduce a comprehensive framework to measure the quality of the generated time series for financial modeling. For example, financial markets have episodes of high and low market volatility. Once in a high (low) volatility market episode, it is expected that the market stays in the high (low) volatility episode for certain period of time. This phenomenon is called volatility clustering. It is important that the forecast of return distribution be conditional on the volatility regime as well as other market information. For this study, only models that generate conditional distribution are considered. The key performance indicators (KPIs) for model comparison cover distribution distance, autocorrelation and backtesting. More details are given in Section 4. Model testing results are presented in Section 4, and we conclude in Section 5.

2 Methodology review

This study covers three categories of models for forecasting (or simulating) future distribution of risk factors.

- The first category is historical simulation, which is widely used by commercial banks for forecasting short term distributions for VaR purpose. This category includes plain historical simulation and improved filtered historical simulation (FHS).
- The second category is parametric models. This category includes widely used parametric models such as autoregressive models (AR), GARCH, Vasicek model and the popu-

<https://www.forbes.com/sites/forbestechcouncil/2023/04/24/fake-accounts-and-fake-data-the-good-the-bad-and-the-preventable/?sh=680c34886678>

⁵<https://www.risk.net/derivatives/equity-derivatives/7921526/jp-morgan-testing-deep-hedging-of-exotics>

lar Nelson-Siegel (NS) representation for yield curves (Diebold and Li (2006)). AR and GARCH can be used to model yields or returns, while Vasicek model and NS representation is applied to yield level in general.

- The third category is deep learning models. This category includes the vanilla conditional GAN (CGAN) model, CGAN with Wasserstein distance (CWGAN), CGAN with LSTM layers, Diffusion model, Signature CWGAN model and Time VAE models. Since only conditional models are covered, there is a C (as in CGAN) for conditional in each deep learning model name.

Machine learning, deep learning and neural network are closely related and have been used interchangeably in general. We use machine learning in a narrow sense: it refers to traditional machine learning models with XGBoost and Random Forest as examples. A deep learning model is “deep” when its structure is composed of many layers of neural networks. In this study, machine learning models are not covered, and deep learning and neural networks are used interchangeably.

Due to time constraint, this study does not include transformer deep learning model.

We focus on GANs which reproduce the whole distribution of one or more market observable prices or rates. Recent work on Tail-GANs focuses on generating the tail distribution alone, either of the observable or of portfolios or trading strategies constructed from the observable (Cont et al. (2023)).⁶ Tail distribution-only generation is beyond the scope of this study.

The 14 models covered in this study are listed in Table 1. In Section 2.2, Vasicek model is also discussed. Vasicek model is a continuous time model and has similar properties as an AR(1) model with time series data. In limited model testing, these two models perform similarly. Therefore, only the simpler AR(1) model is listed in Table 1 and included in comprehensive model testing.

Common notations in the paper are collected into Table 2. To introduce terminology on neural networks, a basic neuron representation⁷ is shown in Figure 1. The input to the neuron is x_1, \dots, x_n , which are combined with weights w_i and bias b (or slope and intercept in linear regression) to form the raw output $\sum_{i=1}^n x_i w_i + b$. Since w_i and b can be any real numbers, the raw output may fall outside the expected range for an application (e.g. outside the range [0,255] for pixel values, or [0, 1] for probability estimate). The raw output is passed to an activation function f to convert the raw output into the expected range. The following are several widely used activation functions.

ReLU (rectified linear unit) or positive part

$$f(x) = \max(0, x) \tag{1}$$

⁶We appreciate Prof. Rama Cont for bringing his research to our attention.

⁷Source, <https://jameskle.com/writes/neural-networks-101>

Table 1: List of models

No.	Model Category	Model Name	Note
1	Historical simulation (HS)	PHS	Plain Historical simulation
2	Historical simulation (HS)	FHS	Filtered historical simulation (EWMA)
3	Parametric (PM)	AR	Autoregressive model of order 1 of yields
4	Parametric (PM)	AR_RET	Autoregressive model of order 1 of return of yields
5	Parametric (PM)	GARCH	AR(1)+GARCH-normal model of yields
6	Parametric (PM)	GARCH_RET	AR(1)+GARCH-normal model of return of yields
7	Parametric (PM)	GARCHt_RET	AR(1)+GARCH-t (with t distribution) model of return of yields
8	Parametric (PM)	NS_VS	Nelson-Siegel 3 factor model with Vasicek dynamics
9	Neural network (NN)	CGAN-FC	Conditional GAN with fully connected layers
10	Neural network (NN)	CGAN-LSTM	Conditional GAN with LSTM layers
11	Neural network (NN)	CWGAN	Conditional GAN with Wasserstein loss
12	Neural network (NN)	DIFFUSION	Diffusion model
13	Neural network (NN)	SIG	Signature CWGAN with CNN layers
14	Neural network (NN)	VAE	Conditional Time VAE model

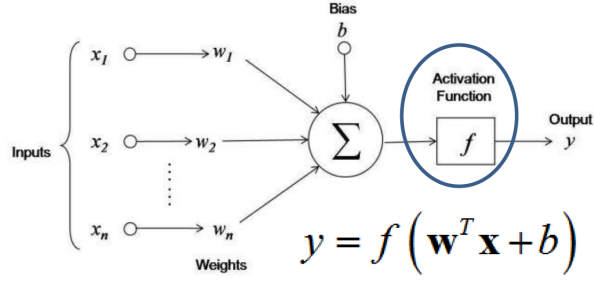


Figure 1: A basic neuron representation

This function converts the raw output from the real line to the positive real line.

Sigmoid or logistic function

$$f(x) = \frac{1}{1 + e^{-x}} \quad (2)$$

This function converts the raw output from the real line to the unit interval $(0, 1)$, appropriate for probability estimates.

Most activation functions are non-linear and inject an element of non-linearity to the neuron. Interestingly, there is a linear activation function that is appropriate for some applications and is used in our study,

$$f(x) = x \quad (3)$$

In our application, the outputs are expected to have mean zero and unit variance and cover the whole real line. A linear activation function is suitable for such cases.

A neural network or deep learning model consists in multiple (and potentially many) neurons side by side (width of a neural network) or sequentially (depth of a neural network) or both, with each neuron having its own weight, bias and activation function. Activation functions for the hidden layers are almost always non-linear.

The representation in Figure 1 is for a basic neuron. There are enhanced representations for special applications, for example, convoluted neural network (CNN) for image application and long short-term memory (LSTM) for recurrent data including natural language processing (NLP) and time series application.

2.1 Historical simulation models

Historical simulation (HS) and the improved filtered historical simulation (FHS) are widely used by commercial banks for VaR models. They are simple nonparametric models that use empirical distribution for distribution forecast.

Table 2: List of notations and model parameters

Notation	Meaning
t	Date of the scenario
d	Number of risk factors in multivariate time series
R_t	Level of d -dimensional risk factor at time t
$R_t(\tau)$	Convenient representation of yield curve. Level of risk factor (yield) of tenor τ at time t . The number of different τ values is d .
$R_t^{(i)}$	Level of risk factor i or tenor $\tau_i, i \in \{1, 2, \dots, d\}$ at time t
\tilde{R}_t	Synthetic level produced by generative model for d -dimensional risk factor and time t
x_t	Return of d -dimensional risk factor at time $t, x_t = R_t - R_{t-1}$.
$x_{t,i:j}$	Return x for the period $t + i, \dots, t + j$
\tilde{x}_t	Synthetic return produced by generative model for d -dimensional risk factor and time t
y	Conditions used as input to the generative model
z	Random noise for generative model
G	Generator in GAN
D	Discriminator in GAN
σ_t	Volatility of return for date t
$\tilde{\sigma}_t$	Volatility forecast of return for date t
ε_t	White noise for date t
P_r	Real data distribution
P_g	Synthetic (generated) data distribution
$E[\dots]$	Expectation of a variable/function

2.1.1 Plain Historical Simulation (PHS) model

In the historical simulation (HS) model, we draw daily returns from the empirical distribution (or empirical distribution function (EDF))⁸. It is simple to implement and naturally takes into account the correlation (and more general forms of dependence) among variables. It is widely used by commercial banks for their VaR models, (Perignon and Smith (2010)).

EDF is an estimate of the distribution that generates the data and converges to the underlying distribution under certain assumptions⁹. However, EDF is an estimate of the unconditional distribution of the data, and does not take into account the serial dependence (over time) in the data. For example, there are regimes of high volatility and low volatility in financial markets. Volatility regimes tend to be persistent in the sense that the market does not switch from high to low volatility regimes daily. Once in a regime, the market tends to stay in that regime for a period of time. If we know that the market is in a high volatility regime today, then in the next few days, the market tends to stay in the high volatility regime. This volatility clustering is captured by the widely used GARCH volatility model, and can be used to improve the distribution forecast, which is the idea behind the filtered historical simulation (FHS) model. To differentiate from FHS, this simple HS is called plain HS (PHS).

HS for one day horizon is straightforward, while HS for multiple day ahead scenario is not obvious. The mechanics of HS is described below.

For a given business date t_0 , a sample of daily returns of size 251 for $t_0 + 1$ from EDF is formed using daily returns of previous 251 days: $x(t_0 - i)$, $i = 0, 1, \dots, 250$ ¹⁰. In this paper, an year is assumed to have 251 business dates. It is common to use 250 and 252 business dates as well.

Similarly, a sample of two-day returns of size 251 for period $(t_0, t_0 + 2)$ from EDF is formed using previous 251 points of overlapping two-day returns: $x(t_0 - i, 2)$, $i = 0, 1, \dots, 250$. For this illustration, the notation is abused a little bit when the second index is used to indicate the returns horizon ($x(t_0 - i, 2)$ for 2-day return), which is the sum of two daily returns. The two day return is calculated as $x(t_0 - i, 2) = x(t_0 - i) + x(t_0 - i - 1)$. See Table 3 for an illustration.

By this example, a one day return for $t_0 + 1$ is $x(t_0 - i, 1) = x(t_0 - i)$, a two day return for period $(t_0, t_0 + 2)$ is $x(t_0 - i, 2) = x(t_0 - i - 1) + x(t_0 - i)$. By this logic, a one day (“forward”) return for date $t_0 + 2$ is naturally taken as the difference between the two-day return and the one-day return above, namely, $x(t_0 - i, 2) - x(t_0 - i) = x(t_0 - i - 1)$, $i = 0, 1, \dots, 250$. See Table 3 again for an illustration.

Selection of scenarios for dates $t_0 + 1$, $t_0 + 2$ and $t_0 + 3$ is illustrated in Table 4, with each row in the table representing a simulation path. The benefit of HS is that it is easy to implement, and is not limited by dimensionality of the data. The drawback is that it is limited to historical

⁸Or empirical cumulative distribution function (ECDF)).

⁹See http://faculty.washington.edu/yenchic/17Sp_403/Lec1_EDF.pdf

¹⁰Due to data processing delays, the time window for selecting the historical scenarios for a bank may not be the most recent 251 days. For example, the time window could be $t_0 - 251, \dots, t_0 - 1$.

Table 3: Illustration of historical simulation for 1-day and 2-day returns

Scenario	Future date		
	$t_0 + 1$	$t_0 + 1$	$t_0 + 2$
	1-day	2-day	1-day (implied)
1	$x(t_0)$	$x(t_0 - 1) + x(t_0)$	$x(t_0 - 1)$
2	$x(t_0 - 1)$	$x(t_0 - 2) + x(t_0 - 1)$	$x(t_0 - 2)$
3	$x(t_0 - 2)$	$x(t_0 - 3) + x(t_0 - 2)$	$x(t_0 - 3)$
4	$x(t_0 - 3)$	$x(t_0 - 4) + x(t_0 - 3)$	$x(t_0 - 4)$
5	$x(t_0 - 4)$	$x(t_0 - 5) + x(t_0 - 4)$	$x(t_0 - 5)$

(return) scenarios. It can be seen in Table 4 that HS scenarios are just historical data in reverse order of time. As a result, it is expected to capture autocorrelation, dependence across tenors and distribution of historical returns.

Table 4: Illustration of historical simulation for 1-day returns

Scenario	Future date		
	$t_0 + 1$	$t_0 + 2$	$t_0 + 3$
1	$x(t_0)$	$x(t_0 - 1)$	$x(t_0 - 2)$
2	$x(t_0 - 1)$	$x(t_0 - 2)$	$x(t_0 - 3)$
3	$x(t_0 - 2)$	$x(t_0 - 3)$	$x(t_0 - 4)$
4	$x(t_0 - 3)$	$x(t_0 - 4)$	$x(t_0 - 5)$
5	$x(t_0 - 4)$	$x(t_0 - 5)$	$x(t_0 - 6)$

2.1.2 Filtered Historical Simulation (FHS) model

FHS takes into account volatility clustering and generates improved conditional distribution forecasts with volatility scaling. The idea is simple (BARONE-ADESI and GIANNOPOULOS (2001)):

1. For given historical market data R_t , calculate returns x_t and estimate of volatility σ_t for each date t . Volatility estimate can be from a generalized autoregressive conditional heteroskedasticity (GARCH) model or exponentially weighted moving average (EWMA) model. GARCH model is described later in Section 2.2.3. For EWMA, see the well known VaR website ¹¹.
2. Calculate devolatilized (devol) return $\hat{x}_t = x_t/\sigma_t$
3. For the problem of forecasting next day conditional distribution at a given business date t_0 , make a forecast of volatility for next day $\tilde{\sigma}_{t_0+1}$

¹¹Value at Risk Theory and Practice, <https://www.value-at-risk.net/exponentially-weighted-moving-average-ewma/>.

4. Select 251 historical devol scenarios in the previous year $\hat{x}_{t_0-i}, i = 0, 1, \dots, 250$
5. Revolatize the selected scenarios $\tilde{x}_{t_0}^i = \hat{x}_{t_0-i}\tilde{\sigma}_{t_0+1}, i = 0, 1, \dots, 250$
6. $\tilde{x}_{t_0}^i$ is a set of 251 data points that form the EDF for date $t_0 + 1$.

Note that FHS involves devol (#2) and revol (#5) steps, which are key steps for capturing volatility persistence. In the devol step, raw returns are standardized for volatility to form a pool of (nearly) i.i.d. returns for future scenarios. In the revol step, the selections from the scenario pool is scaled by future volatility forecast, so that if the market is in a high (low) volatility regime, the i.i.d. scenarios are scaled up (down).

FHS is a simple form of conditional model with the conditional variance estimated with EWMA or GARCH model. Similar to Table 4, selection of scenarios for FHS is illustrated in Table 5.

Table 5: Illustration of filtered historical simulation (FHS) for 1-day returns

Scenario	Future date		
	$t_0 + 1$	$t_0 + 2$	$t_0 + 3$
1	$\hat{x}(t_0)\tilde{\sigma}(t_0 + 1)$	$\hat{x}(t_0 - 1)\tilde{\sigma}(t_0 + 2)$	$\hat{x}(t_0 - 2)\tilde{\sigma}(t_0 + 3)$
2	$\hat{x}(t_0 - 1)\tilde{\sigma}(t_0 + 1)$	$\hat{x}(t_0 - 2)\tilde{\sigma}(t_0 + 2)$	$\hat{x}(t_0 - 3)\tilde{\sigma}(t_0 + 3)$
3	$\hat{x}(t_0 - 2)\tilde{\sigma}(t_0 + 1)$	$\hat{x}(t_0 - 3)\tilde{\sigma}(t_0 + 2)$	$\hat{x}(t_0 - 4)\tilde{\sigma}(t_0 + 3)$
4	$\hat{x}(t_0 - 3)\tilde{\sigma}(t_0 + 1)$	$\hat{x}(t_0 - 4)\tilde{\sigma}(t_0 + 2)$	$\hat{x}(t_0 - 5)\tilde{\sigma}(t_0 + 3)$
5	$\hat{x}(t_0 - 4)\tilde{\sigma}(t_0 + 1)$	$\hat{x}(t_0 - 5)\tilde{\sigma}(t_0 + 2)$	$\hat{x}(t_0 - 6)\tilde{\sigma}(t_0 + 3)$

2.2 Parametric models

Another widely used simulation framework is based on Monte Carlo approach. Each model herein can be written in a parametric form with a theoretical distribution or fixed moving process, governed either by stochastic dynamics or time series. We explore a number of popular parametric models. We use these as benchmarks/challenge models against the neural network models. In the subsequent context, we simply specify the marginal dynamics of a single risk factor for simplicity, i.e. we use R_t and x_t instead of $R_t^{(i)}$ and $x_t^{(i)}$. The correlation of different risk factors can be established through the standard Gaussian copula approach for returns or random noise.

2.2.1 Vasicek model

The Vasicek model is a mean-reverting stochastic process (Vasicek (1977)). It has a long history of applications for interest rate movements and fixed-income risk factor modeling in mathematical finance.

The Vasicek model is usually used to model stochastic process with mean reverting behavior, for example, the level of interest rates.

The Vasicek model specifies the following stochastic differential equation (SDE) of R_t .

$$dR_t = \kappa(\theta - R_t)dt + \sigma dW_t \quad (4)$$

where $\kappa > 0$ is the mean-reverting speed, θ is the long-term mean level of R_t , and σ is the volatility of the Brownian motion dW_t . With the initial condition R_0 given and without loss of generality, for an even partition over $(0, T]$: $0 = t_0 < t_1 = \delta < t_2 = 2\delta < \dots < t_n = n\delta = T$, the SDE (4) can be solved iteratively as the following.

$$R_{i+1} = R_i e^{-\kappa\delta} + \theta(1 - e^{-\kappa\delta}) + \sigma \sqrt{\frac{1 - e^{-2\kappa\delta}}{2\kappa}} z_{t+1} \quad (5)$$

where $R_i = R_{t_i}$ and z_{t+1} is a random sample from standard normal distribution.

Note that in simulation process, the parameters κ, θ, σ are first calibrated from historical data, for instance based on maximum-likelihood estimate (see [van den Berg \(2011\)](#)), and then plugged into equation (5) for future path generation with pre-defined δ , which could be 1-day, 2-day etc. In the multi-dimensional case, i.e. there are a number of risk factors $R^{(1)}, R^{(2)}, \dots, R^{(d)}$, the correlation among these factors needs to be factored in the vector version of equation (5) by correlating d iid samples drawn from $N(0, 1)$ to form the noise vector.

2.2.2 Autoregressive (AR) model

In statistics, econometrics and signal processing, an autoregressive (AR) model is a representation of a type of random process; as such, it is used to describe certain time-varying processes in nature, economics, behavior, etc. The autoregressive model specifies that the output variable depends linearly on its own lagged values and on a stochastic term (an imperfectly predictable term); thus the model is in the form of a stochastic difference equation.

The autoregressive model is usually used to model stationary time series, for example, financial returns.

The notation $AR(p)$ indicates an autoregressive model of order p . The $AR(p)$ model is defined as:

$$x_t = \phi_0 + \sum_{i=1}^p \phi_i x_{t-i} + \varepsilon_t \quad (6)$$

where ϕ_1, \dots, ϕ_p are the parameters of the model, and $\varepsilon_t \sim N(0, \sigma^2)$ is white noise. Here again, the $\{\phi\}_{i=1}^p$ are calibrated from historical time series data and used for future simulation. When $p = 1$, the model is simplified to the popular AR(1) model,

$$x_t = \phi_0 + \phi_1 x_{t-1} + \varepsilon_t \quad (7)$$

To assess the relationship between the above AR(1) model and Vasicek model, assume an

AR(1) for R_t and rewrite (7) for R_t into the following.

$$R_t - R_{t-1} = \underbrace{(1 - \phi_1)}_{\kappa dt} \left(\underbrace{\frac{\phi_0}{1 - \phi_1}}_{\theta} - R_{t-1} \right) + \underbrace{\sigma_{\varepsilon_t}}_{\sigma \sqrt{dt}} Z_t \quad (8)$$

Compared with Vasicek model (4), it is easy to see (8) is special a case of (4) with $\kappa dt = 1 - \phi_1$, $\theta = \frac{\phi_0}{1 - \phi_1}$, and $\sigma \sqrt{dt} = \sigma_{\varepsilon_t}$. But note that this equivalence is under the assumption that dt can be set to 1 day. However dt in differential form (4) should be infinitesimally small in the sense of calculus. Therefore the following distinctions should be made between Vasicek and AR(1):

- The Vasicek model is a general continuous-time model while AR(1) is a typical time-series model in discrete time.
- In view of (8), when $\phi_1 = 1$, it is still an AR(1) model but it no longer satisfies the assumption of a Vasicek model. In fact, with $\phi_1 = 1$, it is a unit root process (Dickey and Fuller (1979)), which is a random walk in discrete time and nonstationary. For modeling, a unit root process is usually converted to a stationary process first, for example, by calculating returns.
- Following further with the point above, when $\phi_1 > 1$, the Vasicek model would break as $\kappa < 0$. Instead of mean-reverting, it becomes mean-avoiding (if the random variable is above the mean, it increases, moving further away from the mean) so that the solution (5) is divergent (or explosive).

In model testing later, Vasicek and AR(1) models have similar performance. For such comparison, Vasicek and AR(1) models are used to model the same variable, which is R_t . The simpler AR(1) model is selected for further comparison with other models.

2.2.3 GARCH model

For AR(1) model (7), it is assumed that the error variance σ^2 is constant. The autoregressive conditional heteroskedasticity (ARCH) model is a statistical model for time series data that describes the variance of the current error term (or innovation) as a function of the actual sizes of the previous time periods' error terms. The ARCH model is appropriate when the error variance in a time series follows an autoregressive (AR) model; if an autoregressive moving average (ARMA) model is assumed for the error variance, the model is a generalized autoregressive conditional heteroskedasticity (GARCH) model. See Engle (1982) and Bollers-

slev (1986). In general, the $GARCH(p, q)$ has the following specification:

$$\varepsilon_t \sim N(0, \sigma_t^2) \quad (9)$$

$$\sigma_t^2 = \omega + \sum_{i=1}^q \alpha_i \varepsilon_{t-i}^2 + \sum_{i=1}^p \beta_i \sigma_{t-i}^2 \quad (10)$$

where $\omega, \alpha_i, \beta_i$ are constants to be calibrated. In applications, $GARCH(1,1)$ model with $p = 1$ and $q = 1$ often works quite well. In this case, combining equations (6) and (10) yields the $AR(1) + GARCH(1, 1)$ model below.

$$\begin{cases} x_t = \phi_0 + \phi_1 x_{t-1} + \varepsilon_t; \\ \varepsilon_t = \sigma_t Z_t, Z_t \sim N(0, 1) \\ \sigma_t^2 = \omega + \alpha \varepsilon_{t-1}^2 + \beta \sigma_{t-1}^2 \end{cases} \quad (11)$$

Note that $AR(1) + GARCH(1, 1)$ is a good benchmark to Vasicek model in that it enables a version of stochastic volatility. The autoregressive nature of conditional variance in $GARCH$ captures volatility clustering in financial time series.

2.2.4 Nelson-Siegel yield curve representation

The Nelson-Siegel (NS) representation of a curve is used for yield curve modeling in financial markets. Instead of being named a model, it is indeed a representation of yield curves $R_t(\tau)$ in term structure (τ) dimension rather than the evolution process in time dimension as in 2.2.1 and 2.2.3. A curve $R_t(\tau)$ is approximated with parameters $\beta_0, \beta_1, \beta_2, \lambda$ as the following (Nelson and Siegel (1987) as reformulated in Diebold and Li (2006)),

$$R_t(\tau; \lambda) \approx \beta_0 + \beta_1 \left(\frac{1 - e^{-\frac{\tau}{\lambda}}}{\tau/\lambda} \right) + \beta_2 \left(\frac{1 - e^{-\frac{\tau}{\lambda}}}{\tau/\lambda} - e^{-\frac{\tau}{\lambda}} \right) \quad (12)$$

Here the four parameters $\beta_0, \beta_1, \beta_2, \lambda$ are calibrated for any given curve with term structure $R_t(\tau_i), i = 1, 2, \dots, d$ on date t . The rationale of approximation (12) relies on the fact that it captures the key attributes of a curve such as level, slope and curvature. In addition, with $\beta_0, \beta_1, \beta_2, \lambda$ known, it is straight-forward to obtain $R_t(\tau)$ for any value τ . To highlight the dependence of $\beta_0, \beta_1, \beta_2$ on time t , (12) is rewritten as

$$R_t(\tau; \lambda) \approx \beta_{0t} \underbrace{f_0(\tau)}_{f_1(\tau)} + \beta_{1t} \underbrace{\left(\frac{1 - e^{-\frac{\tau}{\lambda}}}{\tau/\lambda} \right)}_{f_2(\tau)} + \beta_{2t} \underbrace{\left(\frac{1 - e^{-\frac{\tau}{\lambda}}}{\tau/\lambda} - e^{-\frac{\tau}{\lambda}} \right)}_{f_2(\tau)} \quad (13)$$

where $f_0(\tau) \equiv 1$. In this representation, $\beta_{0t}, \beta_{1t}, \beta_{2t}$ are the three factors, and $f_0(\tau), f_1(\tau)$ and $f_2(\tau)$ are the factor loadings on tenor τ . The three factor loadings are plotted in Figure 2. $f_0(\tau)$ is the loading for a level factor, with $f_1(\tau)$ the loading of a slope factor and $f_2(\tau)$ the loading

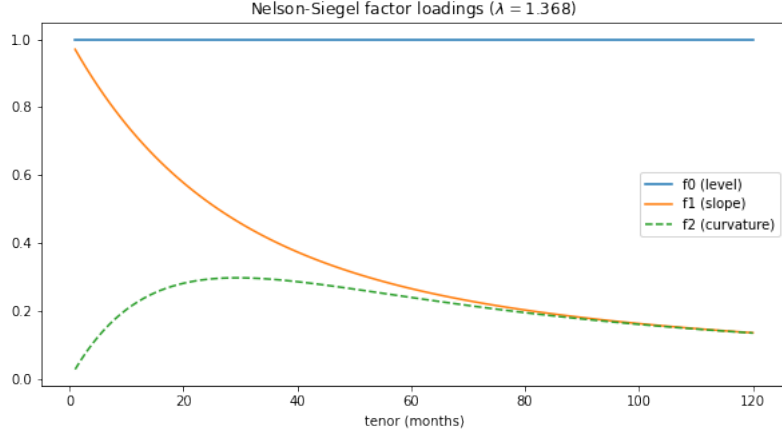


Figure 2: Nelson-Siegel factor loadings

for a curvature factor.

As noted in [Diebold and Li \(2006\)](#), λ affects the decay rate of the slope and the peak of the curvature $f_2(\tau)$. λ is calibrated so that the curvature loading is maximized at 30 months. A benefit of fixing λ to a value (not time variant) is that the other parameters $\beta_{0t}, \beta_{1t}, \beta_{2t}$ can be estimated with OLS. This is a common practice followed in several studies ¹².

A direct usage of Nelson-Siegel representation is similar to PCA (principal component analysis) in the sense that the original curve R_t has d tenors and the approximated R_t only has three parameters (λ is often fixed and not calibrated). When $d > 3$, this is a reduction in dimension in the simulation of R_t . With historical yield curve data, the parameters $\beta_{0t}, \beta_{1t}, \beta_{2t}$ can be calibrated for every date t . Dynamics of these parameters can be modeled using Vasicek model (5) or $AR + GARCH$ model (11). Once the parameters are simulated for a future period, the yield curve $R_t(\tau)$ can be simulated through Nelson-Siegel representation. In this study, Nelson-Siegel representation is applied to the yield curve in levels.

Model testing results show that NS representation with Vasicek dynamics for the factors $\beta_{0t}, \beta_{1t}, \beta_{2t}$ performs better than that with $AR+GARCH$ dynamics. Therefore, for model testing in Section 4, only NS with Vasicek dynamics is presented in model comparison.

2.3 Deep generative models

Given samples from a data distribution, our goal is to generate synthetic data as close to the real data distribution as possible. The key methodology lies in the way the distance between two probability distributions is quantified. Based on the approach to measuring the data distribution, deep generative models can be widely categorized as likelihood-based and likelihood-free models. Among the NN models considered, variational autoencoder (VAE) and Diffusion

¹²Our notation is slightly different from the notation in [Diebold and Li \(2006\)](#). $\lambda = 1/\lambda^*$ (in the reference paper). In the paper $\lambda^* = 0.069$. However, the reference paper uses tenor in months, converting to using annual tenor, $\lambda^{*M} \tau^M = [\lambda^{*M} * 12] \tau^Y = [0.069 * 12] \tau^Y = 0.7308 \tau^Y$. In our study, $\lambda = 1/0.7308 = 1.368$.

models are examples of likelihood-based models, while GAN is a unique likelihood-free model.

GAN is inspired by game theory: the two models, a generator and a discriminator, compete with each other via an adversarial training process. We use conditional GAN (CGAN) to learn conditional distributions in our study. The generator learns to produce samples that resemble real data, while the discriminator is simultaneously trained to distinguish between real and synthetic samples. As the two models are trained together in a zero-sum game, improvements to one model come at the expense of the other model. It is thus challenging to train a GAN model and it may suffer from issues of mode collapse and vanishing gradients. To address the issues with GAN training, WGAN was proposed using Wasserstein distance as an alternative loss function. There are also variations in GAN with different architectures in the generator and discriminator. In LSTM CGAN (LSTM for short), the generator adopts an encoder-decoder structure to capture the volatility dynamics and more complex autocorrelation structures in time series. Signature Conditional Wasserstein GAN (SIGCWGAN) uses an autoregressive network for the generator and uses the mean squared error (MSE) distance between signatures of real and synthetic data as the discriminator.

Besides likelihood-free models, we also evaluate likelihood-based models including VAE and diffusion models. The idea of VAE is to learn a low-dimensional latent representation of the training data called latent variables (variables which can not be directly observed but are rather inferred through a mathematical model), which we assume to have generated our actual training data. Diffusion model is inspired by non-equilibrium thermodynamics. Diffusion model maps data to noise through the successive addition of Gaussian noise in the forward process, and iteratively removes noise in the reverse process. New samples are generated by simply passing randomly sampled noise through the learned denoising process.

A simple way to characterize likelihood-free and likelihood-based models is that likelihood-free models do not take into account the statistical property in the data and just treat the data similar to images, while likelihood-based models utilizes the statistical properties in the data.

We use historical data as continuous conditions to all deep generative models evaluated in this paper. Some of the continuous conditions significantly enhance the model performance on financial time series. Some previous papers for generative models directly use levels of financial time series (such as stock prices and trading volume) for training and generation [Desai et al. \(2021\)](#); [Srinivasan and Knottenbelt \(2022\)](#). In our study, we calculate arithmetic returns or log returns from levels (as discussed in section 3), and model returns in all deep generative models. The usage of returns is more appropriate for financial time series than levels, as returns are more stationary than levels and more widely used in financial applications. We provide a brief summary of deep generative models covered in our study below.

The three groups of deep learning models (GAN, VAE and Diffusion) are described below. For a preview of the size of the neural networks fitted to USD Libor curve data, the number of model parameters are presented in Table 6.

Table 6: Number of model parameters for USD Libor dataset

Model	GEN/DEC	DIS/ENC	TOTAL	Code Library
CGAN-FC	137,434	112,385	249,819	Tensorflow
CWGAN	797,658	158,465	956,123	Torch
DIFFUSION	39,279	0	39,279	GluonTS
CGAN-LSTM	9,929	8,262	18,191	Tensorflow
SIG	11,612	1,781,730	1,793,342	Torch
VAE	86,316	156,420	242,736	Tensorflow

To facilitate discussion of model architecture, the data structure for deep learning model is described first.

2.3.1 Data structure

Imaging application is an important use case for the development of deep learning models and helps to shape the deep learning models for later applications. For an application, the image size is usually fixed. For example, images in the well known MNIST ¹³ image dataset are of fixed size 28×28 . The setup of neural network for financial time series follows image application. Since deep learning models usually expect a dataframe or sequence of a fixed size, time series data in 2-dimensional arrays are sliced into time windows of fixed size. For a typical model in the paper, the 9-tenor USD yield curve ¹⁴ is sliced (or windowed/sequenced) into windows of 20 business dates. Each sequence is a 2-dimensional array (of dimension 20×9), which is similar to an image in deep learning models for imaging applications. This is called sliding or rolling windows (of length 20) in statistical modeling. Concatenating all sequences to an array forms a 3-dimensional array, which are used in model fitting. The first 10 days in the sequence are used as condition and the second 10 days in the window are used as target for prediction (or “label” for supervised learning). The 3-dimensional array is similar to a collection of images. Each 2-dimensional array (20×9) is called a dataframe, a window, a slice or a sequence. In general, a sequence is of dimension $(p + q) \times d$, with p the condition length, q the target sequence length, and d the number of time series (features). For USD yield curve application in this study, $p = 10$, $q = 10$, $d = 9$.

2.3.2 GAN Models

2.3.2.1 CGAN FC A CGAN method is developed and tested by Fu et al. (2019) for multidimensional financial time series generation, where the conditions can be both categorical and continuous random variables. Similar to GAN, CGAN is also a minmax game (14) on a cost function between generator (G) and discriminator (D), where both G and D are neutral

¹³See <http://yann.lecun.com/exdb/mnist/>.

¹⁴For any business date, there are nine interest rates for different maturities. An yield curve is defined as yield (interest rate) as a function of time to maturity or tenor.

network models. The inputs of G are z and y , where z is a random variable from uniform or Gaussian distribution, and y is the condition variable. \mathbb{P}_r is the real data distribution and \mathbb{P}_g is the model distribution implicitly defined by $\tilde{x} = G(z, y)$

$$\minmax_G D \mathbb{E}_{x \sim \mathbb{P}_r} [D(x, y)] + \mathbb{E}_{\tilde{x} \sim \mathbb{P}_g} [\log(1 - D(\tilde{x}, y))] \quad (14)$$

For the training of the discriminator D, the objective is to identify the correct label (True/False) of the data, making $D(\tilde{x}, y)$ ¹⁵ close to zero for synthetic (fake) data, and $D(x, y)$ close to 1 for real data, thus maximizing the loss function. For the training of the generator G, the objective is to fool the discriminator, and make $D(\tilde{x}, y)$ ($\tilde{x} = G(x, y)$) close to 1 for synthetic (fake) data, thus minimizing the loss function. This explains the minmax notation in the loss function (14).

Here the conditions y and noises z are non-linearly mapped to the outputs by multiple fully connected layers with ReLU activation functions for both generator and discriminator in CGAN. A clipping method is used in discriminator to stabilize the training process against spikes in the weights of the neural network layers. Both simulation studies and empirical back-testing show promising model performance for various autocorrelation structure and volatility dynamics [Fu et al. \(2019\)](#).

CGAN FC refers to CGAN with fully connected layers.

2.3.2.2 CGAN LSTM In the previous sub-sections, we introduced the usage of CGAN in time series generation, which is conditional on given historical data. These historical data are added into the generator of CGAN with the noise variables by fully connected layers with ReLU activation functions in general. In the previous studies [Fu et al. \(2019\)](#), we found that the proposed CGAN structure is relatively more sufficient for AR types of time series with simple autocorrelation structures, while it may be challenging to learn the volatility dynamics as GARCH type time series. In order to capture the volatility dynamics and more complex autocorrelation structures, we propose an encoder-decoder structure for the generator of CGAN. The encoder is trained to convert conditional raw data into required information, and the decoder is trained to decode the trained conditions and use it to generate the conditional outcomes. We propose to use separate LSTM layers ([Yu et al. \(2021\)](#)) for both encoder and decoder in the generator. The LSTM layers capture both long- and short-term dependences and generate sequence outputs with shared weights along time, which is a natural choice for time series generation. We only use single-direction LSTM in the generator, as the time series is generated along the forward time direction. There are two LSTMs used in G, where the first LSTM takes the conditions as inputs and generate the long- and short-term state variables as the initial state variables of the second LSTM. Suppose the conditions are from x_1, \dots, x_T , then for $t \in [1, T]$, and a typical LSTM cell has three gates: input, forget, and output, which decide whether or not to allow new input in, forget old information, and affect output at current

¹⁵Note that y appears twice in the formula. $\tilde{x} = G(z, y)$ shows the conditional generator and $D(G, y)$ shows the conditional discriminator.

time-step (Yu et al. (2021)).

$$i_{1,t} = \sigma(w_{1,i}[a_{1,t-1}, x_t] + b_{1,i}) \quad (15)$$

$$f_{1,t} = \sigma(w_{1,f}[a_{1,t-1}, x_t] + b_{1,f}) \quad (16)$$

$$o_{1,t} = \sigma(w_{1,o}[a_{1,t-1}, x_t] + b_{1,o}) \quad (17)$$

$$\tilde{c}_{1,t} = \tanh(w_{1,c}[a_{1,t-1}, x_t] + b_{1,c}) \quad (18)$$

$$c_{1,t} = i_{1,t} \cdot \tilde{c}_{1,t} + f_{1,t} \cdot c_{1,t-1} \quad (19)$$

$$a_{1,t} = o_{1,t} \cdot \tanh(c_{1,t}) \quad (20)$$

where $i_{1,t}$, $f_{1,t}$ and $o_{1,t}$ denote the input, forget and output gates of the first LSTM respectively. $a_{1,t}$ is the short-term state variable, while $c_{1,t}$ is the long-term state variable passing along the time in the first LSTM layer training process. $w_{1,\cdot}$'s and $b_{1,\cdot}$'s are the weights and biases of the first LSTM. The first LSTM will process the conditions x_1, \dots, x_t , and output the final long- and short-term state variable $c_{1,T}$ and $a_{1,T}$. $a_{1,T}$ is also the ultimate output of the LSTM layer.¹⁶

The second LSTM takes $c_{1,T}$ and $a_{1,T}$ as the initial state variables, and takes noises z_1, \dots, z_S , as inputs to generate real-like outputs of the time series.

Under the LSTM-CGAN structure, the discriminator leverages LSTM layers in order to compete with the generator with LSTM layers. For the time series y_1, \dots, y_{S+T} from either real or generated data, the discriminator LSTM has a similar structure to the LSTM layers discussed above. More details of the structure are given in Appendix. The training process follows the same minmax game and uses the same loss function as CGAN.

2.3.2.3 CWGAN The Wasserstein distance is a distance function defined between two probability distributions P and Q on a given metric space M . If each distribution is viewed as a unit amount of earth (soil) piled on M , the metric is the minimum "cost" of turning one pile into the other, which is assumed to be the amount of earth that needs to be moved times the mean distance it has to be moved. Because of this analogy, the metric is known in computer science as the *earth mover's distance*.

For two empirical distributions P with samples p_1, \dots, p_n and Q with samples q_1, \dots, q_n , the Earth-Mover (EM) or Wasserstein-1 distance is

$$W(P, Q) = \inf_{\gamma \in \Pi(P, Q)} E_{(p, q) \sim \gamma} [\|p - q\|] \quad (21)$$

where $\Pi(P, Q)$ denotes the set of all joint distributions $\gamma(p, q)$ whose marginals are P and Q . For a given p, q the joint distribution $\gamma(p, q)$ tells how much "mass" must be transported from p to q to transform P into Q . The EM distance is then the cost of the optimal transport plan (Arjovsky et al. (2017)). Intuitively, given two distributions, one distribution P can be seen as a mass of earth properly spread in space, the other distribution Q as a collection of holes in

¹⁶The gates serve as latent variables that define the internal structure of LSTM.

that same space. Then, the Wasserstein distance measures the least amount of work needed to fill the holes with earth. $\|p - q\|$ measures the distance between p and q . The infimum is over all permutations of elements in the two distributions. Wasserstein distance is used in both Wasserstein GAN (WGAN) and Signature Conditional Wasserstein GAN (SIGCWGAN).

Generative Adversarial Networks (GANs) are challenging to train, and oftentimes it causes the model convergence issue such as mode collapse and vanishing gradients [Arjovsky et al. \(2017\)](#). To address the issues in GAN training, WGAN was proposed using Wasserstein distance as a new cost function. Compared to GAN, WGAN improves the stability of learning, gets rid of the mode collapse issue, and provides meaningful learning curves useful for debugging and hyperparameter searches [Arjovsky et al. \(2017\)](#). The loss function of WGAN is constructed using the Kantorovich-Rubinstein duality as:

$$\min_G \max_{D \in \mathcal{D}} \mathbb{E}_{x \sim P_r} [D(x)] - \mathbb{E}_{\tilde{x} \sim P_g} [D(\tilde{x})] \quad (22)$$

where \mathcal{D} is the set of 1-Lipschitz functions ¹⁷, P_r is the real data distribution, and P_g is the model distribution implicitly defined by $\tilde{x} = G(z)$, $z \sim N(0, 1)$.

There are two approaches to enforcing the Lipschitz constraint in WGAN: weight clipping and gradient penalty (GP). In our analysis, we evaluate the conditional version of both WGAN and WGANGP, which are CWGAN and CWGANGP, respectively. CWGAN achieves better backtesting performance than CWGANGP. Therefore, only CWGAN is covered in model comparison in this study. CWGAN takes additional conditions y as input to both the generator and critic. For CWGAN, the discriminator is called the critic because the discriminator is no longer a binary classifier (True/False) as in CGAN. The loss function for CWGAN is:

$$\min_G \max_{D \in \mathcal{D}} \mathbb{E}_{x \sim P_r} [D(x, y)] - \mathbb{E}_{\tilde{x} \sim P_g} [D(\tilde{x}, y)] \quad (23)$$

The critic calculates the distance between the real and synthetic data as in (23). We set the clipping threshold to 0.01, so the weights of the critic lie within a compact space $[-0.01, 0.01]$.

2.3.2.4 Conditional Signature Wasserstein GAN Instead of using neural networks to do classification in the discriminator, Signature Conditional Wasserstein GAN (SIGCWGAN, or SIG for short) calculates the distance between the signature of real and synthetic paths as the discriminator. The signature S of a time series sequence X is a nonlinear function $S(X)$ sufficient to capture certain features of the time series (think of principal component analysis as an example). Details of signature and the loss function Conditional Signature Wasserstein-1 metric (C-Sig-W1) are discussed in the appendix.

A model is fitted to predict future signature from the past signature, $S_{t,1:q} = L(S_{t,-p:0})$ with predicted values $\hat{S}_{t,1:q} = \hat{L}(S_{t,-p:0})$. The generator network generates random values of X

¹⁷Explain the meaning of Lipschitz functions.

from past conditions $X_{t,-p:0}$ and random noise Z , $\tilde{X} = G(Z, X_{t,-p:0})$. The generated sample has signature $S(\tilde{X})$. The objective of the generator is to match the expected future signature of synthetic data $E[S(\tilde{X})]$ with the fitted future signature of the actual data $\hat{S}_{t,1:q}$, thus minimizing $(E[S(\tilde{X})] - \hat{S}_{t,1:q})^2$.

The signature function S is given. The first step in training SIGCWGAN is to fit the signature forecast function L . The second step is to optimize the generator G given loss function calculated from signatures of real and synthetic data. Both S and L are given in the fitting of the generator model G . If the fitting of L in the first step is not good, then the optimization in the second step will be optimizing to the wrong target \hat{S} . In the original paper, L is suggested to be a linear function. To improve model fit in the first step and for the overall model, we also implement feed forward (fully connected) networks and CNN as the signature forecast function L .

Note that this is a typical forecast problem for $\hat{S}_{t,1:q}$, only the mean (of the signature of the synthetic and actual distribution) is used, and the distribution itself is not used directly.

Prior to taking the signature $S(X)$ of X , X is *augmented* in the sense of [Morrill et al. \(2020\)](#); [Chevyrev and Kormilitzin \(2016\)](#), with the following transformations: scaling, cumulative sum, and adding lags and leads. These augmentations are intended to normalize and enrich the time series with additional information. This is similar to adding quadratic and interaction terms in regression. We provide one example of the data transformation process in the appendix.

In the case of 9-tenor USD yield curve data, there are 2,824 training sequences which are 20-day windows of returns (rate changes). The first 10 days in the window are used as condition and the second 10 days in the window are used as target for prediction. The condition matrix is of size 10×9 . Applying the augmentations above, we get a matrix of size 3×36 . The augmented matrix of size 3×36 for a single sequence is slightly larger than the input matrix of size 10×9 . There is a depth parameter for augmentation. At depth 1, the signature is of size 36. At depth 2, the signature is of size 1332. At depth 3, the signature is of size 47,988. The size of the signature is highly nonlinear in the depth. The original source for this model, [Sabat  \(2021\)](#), uses depth 2 for most time series. We feel that depth 3 might be hard to fit or lead to overfitting. So our model uses depth 2.

To generate a synthetic time series, the generator G uses an *autoregressive feed-forward neural network* (ARFNN) which is built from layers of *residual blocks* and a forward function that implements the autoregressive behavior. Details of ARFNN configuration are discussed in the appendix.

2.3.3 Likelihood-base deep generative models

2.3.3.1 Variational Autoencoder (VAE) Variational Autoencoder is one of the latent based models [Kingma and Welling \(2019\)](#). A variational autoencoder can be defined as being an autoencoder whose training is regularised to avoid overfitting and to ensure that the latent space has good properties that enable generative process. Other than traditional autoencoder that

provides a point estimate that might cause severe overfitting among input data, the encoder in variational autoencoder constructs a distribution of the embedding in the latent space. The goal of variational autoencoder is a sample that accurately represents the distribution of original data, given input data X that consist of N i.i.d. samples of some continuous or discrete variable x . A two step process is applied. The first step generates value z from prior distribution $p_\theta(z)$, and the second step is to generate value x from conditional distribution or likelihood $p_\theta(x|z)$. Assuming that both the prior $p_\theta(z)$ and likelihood $p_\theta(x|z)$ are differentiable, the VAE is composed of three components: input data, output data and latent space. As such, the encoder is applied to model probabilistic posterior distribution $p_\theta(x|z)$, which is approximated by $q_\phi(z|x)$ to ease computation and ensure tractability, while the decoder is to model the conditional likelihood $p_\theta(x|z)$.

Since latent space is modeled by a distribution, a specific distribution needs to be assumed. In the case of Gaussian Variational Autoencoder, both probabilistic posterior distribution $q_\phi(z|x)$ and prior distribution $p_\theta(z)$ are assumed to be Gaussian.

The loss function of VAE is called Evidence Lower Bound loss function (ELBO) and given in the following formula.

$$L_{\theta,\phi} = -E_{q_\phi(z|x)}[\log p_\theta(x|z)] + D_{KL}(q_\phi(z|x), p_\theta(z)) \quad (24)$$

where the first term $-E_{q_\phi(z|x)}[\log p_\theta(x|z)]$ is the negative log-likelihood of data given z sampled from $q_\phi(z|x)$. The second term $D_{KL}(q_\phi(z|x), p_\theta(z))$ is the KL-Divergence loss between the encoded latent space distribution and the prior.

In our case, we adapt the TimeVAE model (VAE for short) [Desai et al. \(2021\)](#) implementation ¹⁸. This model is an implementation of VAE on time series data, with deep learning layers such as dense and convolutional layers, as well as custom layers to model time-series specific components such as level, trend, and seasonal patterns.

In our study, we further improve VAE with couple of steps listed below.

Network enhancement: LSTM

Other than the existing network structure in VAE [Desai et al. \(2021\)](#) (such as dense, convolutional, trend block, seasonality block, etc), we add LSTM layers which is a good candidate to capture longer time dependency of data, as enhancement to the model.

Continuous conditional VAE

To enable longer horizon generation of synthetic data, a continuous conditional VAE framework is proposed and implemented. The basic idea behind the condition is to take advantage of the most currently available information and concatenate with the input data (either real time series data in encoder or noise input as in the decoder) to make the generated data align better with real data. With the condition y , the loss function of conditional VAE (or CVAE)

¹⁸published on GitHub as <https://github.com/abudesai/timeVAE>

becomes

$$L_{\theta,\phi} = -E_{q_{\phi}(z|x)}[\log p_{\theta}(x|z, y)] + D_{KL}(q_{\phi}(z|x, y), p_{\theta}(z|y)) \quad (25)$$

2.3.3.2 Diffusion Diffusion originates from thermodynamics to describe the moving of particles from regions of higher concentration to lower concentration. In quantitative finance, diffusion appears most commonly in the form of Brownian motion with linearly increasing variance. As a deep learning model, diffusion has constant variance through a variance scheduler β_t as in (29).

Diffusion models have emerged as a powerful class of generative models recently. Well known deployed applications include DALL.E 2, Stable Diffusion and Midjourney. For example, the model can generate realistic images from simple text input such as “vibrant California poppies”¹⁹.

These models generate high quality samples and often outperform generative adversarial networks (GANs) in the challenging task of image synthesis Ho et al. (2020); Dhariwal and Nichol (2021). Diffusion models are a class of latent variable models inspired by considerations from non-equilibrium thermodynamics Ho et al. (2020)²⁰. There are two processes in a diffusion model: a forward process that maps data to noise, and a reverse process that performs iterative denoising. New samples are subsequently generated by first sampling from a simple prior distribution (e.g., standard Gaussian), followed by ancestral sampling through the reverse process.

In the forward process, an image (the data) is converted to noise in N successive steps, $x_0 \rightarrow x_N$. Each step is done through Gaussian normal distributions, also known as forward diffusion kernel (FDK),

$$x_t = \sqrt{1 - \beta_t}x_{t-1} + \sqrt{\beta_t}\epsilon_t, \epsilon_t \sim N(0, 1) \quad (26)$$

$$x_t|x_{t-1} \sim N(\sqrt{1 - \beta_t}x_{t-1}, \beta_t\mathbf{I}) \quad \text{conditional} \quad (27)$$

$$x_t \sim N(0, \mathbf{I}) \quad \text{unconditional} \quad (28)$$

For perspective, (26) can be converted into the usual SDE form (with $dt = 1$):

$$dx_t = - \underbrace{(1 - \sqrt{1 - \beta_t})}_{\kappa_t} x_t dt + \underbrace{\sqrt{\beta_t}}_{\sigma_t} dW_t \quad (29)$$

This is a controlled mean reversion process with mean zero, time varying κ and σ to keep the variance of the process constant.

¹⁹<https://www.unite.ai/diffusion-models-in-ai-everything-you-need-to-know>

²⁰There are three categories of diffusion models, (1) denoising diffusion probabilistic models, (2) noise conditioned score based generative models, (3) stochastic differential equations. <https://www.unite.ai/diffusion-models-in-ai-everything-you-need-to-know/>. See <https://sander.ai/2022/01/31/diffusion.html?ref=assemblyai.com> for informal technical discussion.

The forward process $q(x^{1:N}|x^0)$ is fixed to a Markov chain ²¹ that describes the transition from step $n - 1$ to step n : $q(x_t|x_{n-1})$. It gradually adds Gaussian noise (“corrupting” the data in the noising process) to the data following a variance schedule β_1, \dots, β_N . In our experiment, we follow the practice in TimeGrad [Rasul et al. \(2021\)](#): we set the number of diffusion steps $N = 100$, and use a linear variance schedule starting from $\beta_1 = 1 \times 10^{-4}$ till $\beta_N = 0.1$.

The distribution in the reverse process is denoted as $p_\theta(x^{0:N})$. It is defined as a Markov chain with learned Gaussian transitions starting at $p(x^N) \sim \mathcal{N}(\mathbf{0}, \mathbf{I})$:

$$p_\theta(x^{0:N}) := p(x^N) \prod_{n=N}^1 p_\theta(x^{n-1}|x^n) \quad (30)$$

$$p_\theta(x^{n-1}|x^n) := \mathcal{N}(\mu_\theta(x^n, n), \Sigma_\theta(x^n, n)\mathbf{I}) \quad (31)$$

In this setup, the reverse diffusion kernel (RDK) is also Gaussian. With this reverse Markov chain, we can generate a data sample x^0 by first sampling a noise vector $x^N \sim p(x^N)$, then iteratively sample from the learnable transition kernel $x^{n-1} \sim p_\theta(x^{n-1}|x^n)$ until $n = 1$. The mean and variance of the Gaussian kernel μ_θ and Σ_θ are parameterized by θ and defined by a neural network to be specified later. This is a critical drawback of the diffusion model: it requires iterations through N time steps to produce a high quality sample. It is much slower than GANs, which only needs one pass through a network. As noted in [Song et al. \(2020\)](#), diffusion model takes 20 hours to sample 50k images of size 32×32 , while GAN takes less than a minute. It is consistent with what we observed in our analysis.

The diffusion model we test in our evaluation is TimeGrad, an autoregressive model for multivariate probabilistic time series forecasting. Temporal dynamics are modeled by the autoregressive recurrent neural network (RNN) architecture from [Graves \(2013\)](#); [Sutskever et al. \(2014\)](#). Maximization of the log likelihood of a complex joint distribution has much commonality with VAE. Indeed, for Diffusion model, the log likelihood is also formulated with evidence variational lower bound (ELBO). Details of TimeGrad architectures are discussed in appendix. In training process, we randomly sample context and adjoining prediction sized windows from the training data. The network minimizes the difference between real noise ϵ and predicted noise ϵ_θ for time step t and step index n :

$$\mathbb{E}_{x_t^0, \epsilon, n} [\|\epsilon - \epsilon_\theta(\sqrt{\bar{\alpha}_n}x_t^0 + \sqrt{1 - \bar{\alpha}_n}\epsilon, \mathbf{h}_{t-1}, n)\|^2] \quad (32)$$

where $\alpha_n = 1 - \beta_n$, $\bar{\alpha}_n = \prod_{s=1}^n \alpha_s$. ϵ_θ is the noise predicted from RNN, which takes three inputs: $x^n = \sqrt{\bar{\alpha}_n}x_t^0 + \sqrt{1 - \bar{\alpha}_n}\epsilon$, the hidden state \mathbf{h}_{t-1} , and step index n . In inference step, we sample random noise $x_{T+1}^N \sim \mathcal{N}(\mathbf{0}, \mathbf{I})$ and iterate through N time steps in reverse process to generate a sample x_{T+1}^0 , which is passed autoregressively to the RNN (together with possible covariates

²¹In economic and finance applications, Markov Chain with finite state space is often used in Markov switching model. In the current context, the Markov Chain has infinite uncountable number of states due to the use of normal distribution in each step.

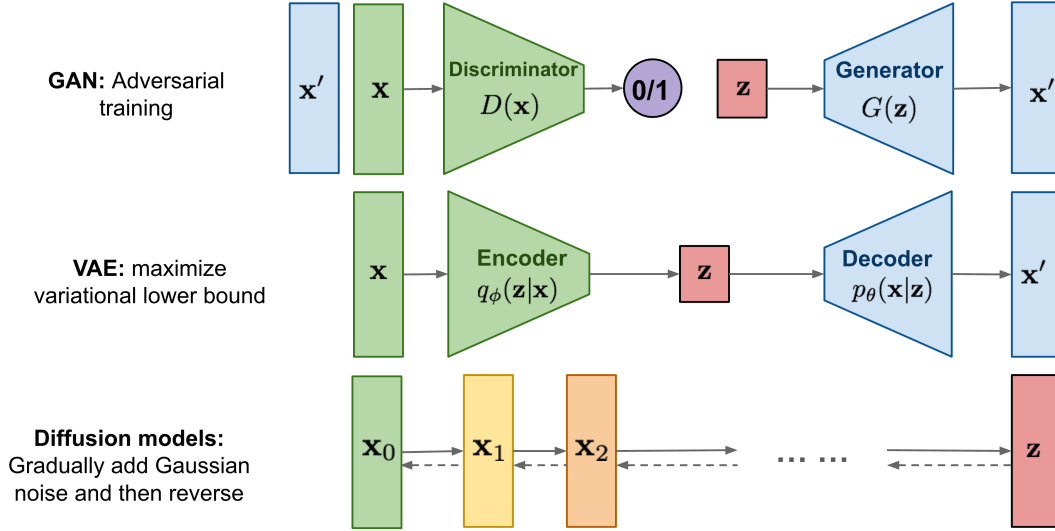


Figure 3: Architecture comparison among three groups of generative models

c_{T+1}) to obtain the next hidden state h_{T+1} . This process is repeated until the desired forecast horizon has been reached.

2.3.4 Network architecture structure

The high-level architecture comparison of the major three groups of deep generative models (GAN, VAE and Diffusion) can be found in Figure 3. There are quite some review work done on GAN models used in time series data, as in Brophy et al. (2021), Brophy et al. (2023). Basically all that generative models do is to build up and train a mapping between input data x and random noise z through different architectures and building blocks, and a generator takes random numbers to generate synthetic samples²².

Given sample data, our goal is to approximate a data distribution as closely as possible. In other words, we have to evaluate and optimize the distance between the data distribution and model distribution. Different approaches can be applied to this end, based on the way to measure distribution distance. One way is likelihood-based models, which seek to learn a model that assigns a high likelihood to the observed data samples. Most of the models in this class apply KL divergence, which is statistically efficient, but requires the ability to evaluate or optimize likelihood tractably. Another approach is likelihood-free inference using adversarial training, which conduct a minmax optimization. Therefore the deep generative models can be widely categorized into two classes: likelihood-based models and likelihood-free models. The loss function of each model reflects the architecture. Table 7 lists the loss functions and explanation of the architecture. The loss functions of different deep generative models measure the distance between real and synthetic data with different approaches.

²²A linear regression model is a trivial case. Let $y = bx + \epsilon$, $\epsilon \sim iidN(0, \sigma^2)$. The mapping from data to noise is $y - bx$, and the generator takes noise ϵ in simulation, $bx + \epsilon$.

Table 7: Loss function of NN models

Model	Loss function	Architecture explained
CGAN (FC, LSTM)	$\min_G \max_D \mathbb{E}_{x \sim \mathbb{P}_r} [D(x, y)]$ $+ \mathbb{E}_{\mathbf{x} \sim \mathbb{P}_g} [\log(1 - D(\mathbf{x}, y))]$	Conditional GAN optimizes two conflicting objective functions at the same time: generator and discriminator.
CWGAN	$\min_G \max_{D \in \mathcal{D}} \mathbb{E}_{x \sim \mathbb{P}_r} [D(x, y)]$ $- \mathbb{E}_{\mathbf{x} \sim \mathbb{P}_g} [D(\mathbf{x}, y)]$	Conditional GAN with Wasserstein loss improves the convergence of GAN. Wasserstein distance has the properties that it is continuous and differentiable and continues to provide a linear gradient.
SIG	$\text{CSigW}_1(\mu, \nu; p, q) =$ $\left \mathbb{E}_{\mathbb{P}_r} [S(X_{t+1:t+q}) x_{t-p+1:t} = x] \right.$ $\left. - \mathbb{E}_{\mathbb{P}_g} [S(\hat{X}_{t+1:t+q}) x_{t-p+1:t} = x] \right $	Signature CWGAN with CNN layers minimizes the summation of the ℓ_2 norm of the error between the conditional expected signature of future real path and future synthetic path generated by the generator with a given condition.
VAE	$L_{\theta, \phi} = -\mathbb{E}_{q_{\phi}(z x)} [\log p_{\theta}(x z, y)]$ $+ D_{KL}(q_{\phi}(z x, y), p_{\theta}(z y))$	Conditional Time VAE model minimizes the reconstruction loss (in real space) and KL-divergence (in latent space) at the same time.
Diffusion	$-\log p_{\theta}(\mathbf{x}^0 \mathbf{x}^1)$ $+ D_{KL}(q(\mathbf{x}^N \mathbf{x}^0), p(\mathbf{x}^N))$ $+ \sum_{n=2}^N D_{KL}(q(\mathbf{x}^{n-1} \mathbf{x}^n, \mathbf{x}^0),$ $p_{\theta}(\mathbf{x}^{n-1} \mathbf{x}^n))$	Diffusion model optimizes KL-divergence between Gaussian distributions. Encoder is predetermined, and the goal is to learn a decoder that is the inverse of this process.

2.4 Single-step vs. multi-step prediction

Traditional time series model such as ARMA predicts the observation at the next time step x_{t+1} given the previous available observations x_{t-k}, \dots, x_t . This is called single step prediction. This is the case with most traditional statistical models, such as AR(1) model (7). Different from traditional time series prediction, deep learning generative models normally work in a sequence-to-sequence approach (Kuznetsov and Mariet (2018); Graves (2013); Sutskever et al. (2014)). Image application is an important use case for the development of deep learning models and helps to shape the deep learning models for later applications. In image generation, the model generates a whole image in one pass, rather than generating the image by part. For time series generation with deep learning model, similar to image generation, it is customary to generate multiple time series covering multiple days in one pass.

Given the shape of training data, specifically the target sequence length of data, deep learning models can generate up to the sequential length of prediction in one sample. As a special case, if the target sequential length q is 1, it is equivalent to single step prediction. Otherwise, if target sequence length is $q > 1$, multistep forecast is generated in one pass, and the first observation in the generated sample can be used as single-step prediction.

It should be noted that the focus of our study is generating distribution forecast of risk factors rather than any point forecast. The forecast is represented by drawing Monte Carlo samples from the underlying probabilistic models, as defined either from real or latent space. With that, the generated samples (or paths) need to be large enough to reasonably describe the distribution of generated sample, and the corresponding quantiles or confidence intervals at any given step.

For the generation of any single path, in a multi-step prediction, the model needs to learn to predict a sequence of future values. Thus, unlike a single-step model, where only a single future point is predicted, a multi-step model predicts a sequence of the values into the future. Given that generative model normally has more than 1 as target sequence length to learn the long term dynamics of data, the generative model normally generates multi-step prediction with any given sample.

For illustration, assume the condition length $p = 10$ and target sequence length $q = 10$, that is, the model uses the previous 10 days to generate forecast for the next 10 days in one pass.

2.4.1 Direct forecast

Consider the case that up to 5 days forecast (forecast horizon=5) is needed. Forecasts up to 10 days are produced by the model in one pass. The first 5 days' forecast satisfy the forecast requirement, and the forecast for days 6 to 10 can be ignored.

2.4.2 Iterative forecast

Consider the case that up to 20 days forecast is required. Using 10 lagged values as conditions $y_0 = x_{t-9:0} = (x_{t-9}, x_{t-8}, \dots, x_t)$, forecast for the first 10 days covering the period $(t+1, \dots, t+10)$, $\tilde{x}_{t,1:10} = G(z, y_0)$ (z is random noise), is generated in one pass of the model. Then using $y_1 = \tilde{x}_{t,1:10}$ as condition, $\tilde{x}_{t,11:20} = G(z, y_1)$ (z is random noise) is generated in another pass of the model. This process can be iterated to generate forecast for longer horizon.

Signature (SIG) model has the built-in autoregressive feature, and can generate long horizon forecast without ad hoc iteration outside the model.

3 Data

Both historical data and simulated data are used for model training and testing.

Since historical data are generated in the real world subject to many factors, its exact property or data generation process (DGP) is unknown. To enhance model testing, we simulate multiple long time series from two well known models: GARCH and CIR (Cox et al. (1985)) model. Both are widely used models for risk factor modeling in finance. The simulated data

have known autocorrelation and conditional variance properties. We can use the simulated data to check whether the models can capture these properties in the data.

In fact, our model testing results show that model performance is indeed different when the data have very fat tails (when simulated data follow GARCH-t(3) distribution). See Section 4.4 for details.

3.1 USD yield curve

Yield curve modeling is an active area of multivariate time series modeling for several reasons, (1) yield curve is the driver for many financial products, (2) there is strong dependence among interest rates of different tenors, i.e., term structure, (3) there is interesting time series dependence for yield curves. USD yield curve (USDYC) is the main data for model development testing. Three USDYC datasets with nine tenors are used. For ease of reference, these three datasets are referred to as USDYC1 (Libor curve 2008-2022), USDYC2 (Par yield 2008-2023) and USDYC3 (Par yield 2000-2023). See more details below.

3.1.1 3 month USD LIBOR curve

This dataset is comprised of 9 typical tenors: 3 month, 6 month, and 1,2,3,5,10,20 and 30 years, of the United States Dollar 3 month LIBOR zero-coupon yield curve, for the business dates ranging from Jan. 2, 2008 to Feb. 5, 2022.

3.1.2 Treasury Par Yield Curve

This is sourced from the Federal Reserve Bank of St Louis (FRED)²³. The dataset covers the period 1990-current date. To fully use the available nine tenor historical data, our model training and testing are done using both 2000-2023 (Jan. 3, 2000 - Feb. 16, 2023) and 2008-2023 (Jan. 2, 2008 - Feb. 16, 2023) time periods.

For ease of reference, these three datasets are referred to as USDYC1 (2008-2022 Libor curve), USDYC2 (Par yield 2008-2023) and USDYC3 (Par yield 2000-2023). USDYC3 is plotted in Figure 4.

3.2 Simulated data for model training and testing

3.2.1 AR(1)+GARCH for rate changes

An AR(1) for conditional mean and GARCH(1,1) for conditional variance is used to simulate data for model testing. This is designed to assess whether the candidate models can capture correlation across tenors, autocorrelation and volatility clustering in the returns. In order

²³<https://fred.stlouisfed.org/>. Also available from Federal Reserve Board's H15 series or Treasury website, <https://home.treasury.gov/policy-issues/financing-the-government/interest-rate-statistics>

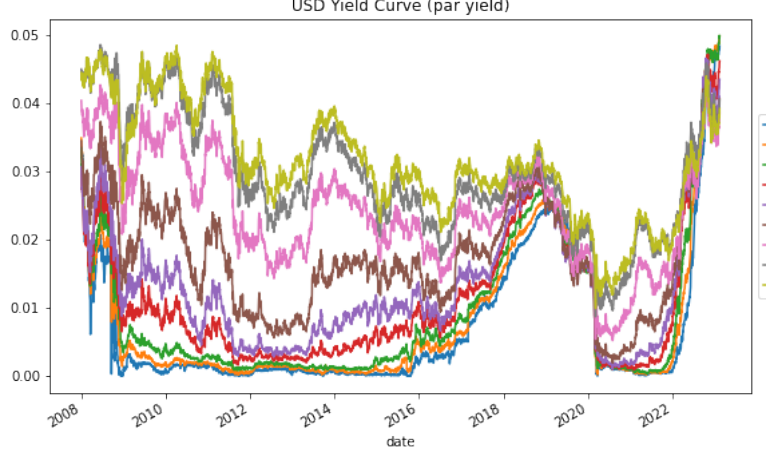


Figure 4: USD Par Yield Curve

to limit the model running time for testing, only bivariate time series are simulated. The simulation model is represented as follows,

$$R_{t+1} = R_t + x_{t+1} \quad (33)$$

$$x_{t+1} = \phi_1 x_t + \epsilon_{t+1} \quad (34)$$

$$\epsilon_{t+1} = \sigma_{t+1} z_{t+1}, z_{t+1} \sim N(0, 1), t(3) \quad (35)$$

$$\sigma_{t+1}^2 = \omega + \alpha \epsilon_t^2 + \beta \sigma_t^2 \quad (36)$$

Bivariate time series is generated from the AR(1)+GARCH(1,1) model with separate parameters for each time series, and correlation between innovations z_t of the two time series. The simulated bivariate time series covers 30 years of daily data (or length of 250×30). For ease of reference, these two time series are called “3m” and “1y” for 3-month and 1-year interest rates. The parameters used in the simulation are presented in Table 8. In the table, ϕ_1 is the autocorrelation in the AR(1) model, ω, α, β are parameters of the GARCH(1,1) model, ρ is the correlation between the innovations of the two time series, Variance is the unconditional variance of the GARCH model ($\omega/(1 - \alpha - \beta)$), and Vol is the unconditional volatility ($\sqrt{\omega/(1 - \alpha - \beta)}$). The parameters are at the scale of interest rates in percentage. For example, 0.029 volatility is 2.9% volatility for daily changes in annualized interest rate.

Param	3M	1Y
ϕ_1	0.5	-0.5
ω	0.000009	0.000012
α	0.1742	0.0724
β	0.8158	0.9176
$\alpha + \beta$	0.9900	0.9900
ρ	0.70	
Variance	0.00086	0.00115
Vol	0.029	0.034

Table 8: Parameters for data simulation from GARCH model

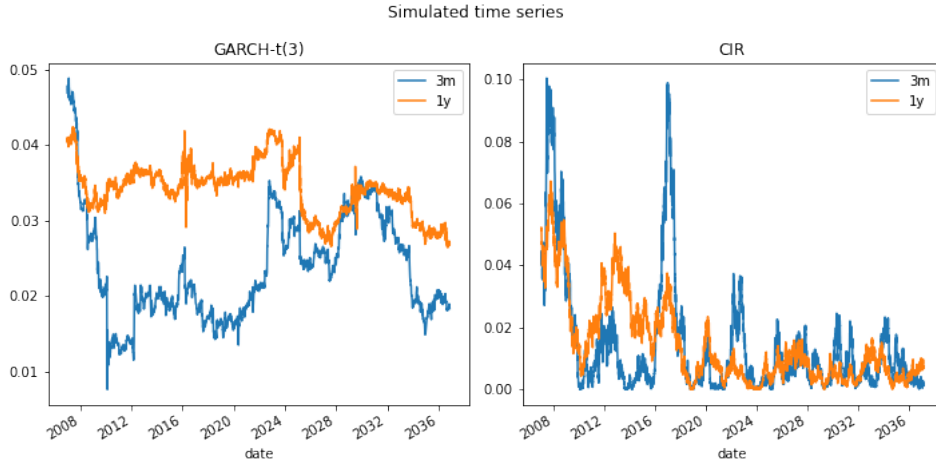


Figure 5: Simulated time series

3.2.2 CIR for Interest Rates

The following typical parameters are used to simulate interest rates data from CIR model,

$$dR_t = \kappa(\theta - R_t)dt + \sigma\sqrt{R_t}dW_t \quad (37)$$

$$\kappa_1 = 0.45, \theta_1 = 0.02, \sigma_1 = 0.15 \quad (38)$$

$$\kappa_2 = 0.20, \theta_2 = 0.03, \sigma_2 = 0.10 \quad (39)$$

$$dW_{1t}dW_{2t} = \rho dt, \rho = 0.60 \quad (40)$$

These are typical parameters calibrated for yield curve. Again bivariate time series of 30 year daily data are simulated, and the same set of parameters are applied for both time series and uncorrelated with each other ²⁴. Selected simulated data are plotted in Figure 5.

²⁴In the simulation algorithm for “exact” distribution with normal distribution and χ^2 distribution as components, it is not clear how to introduce correlation across time series in an intuitive way. To introduce correlation between the two simulated series, simulation uses Euler discretization.

3.2.3 Data preparation pipeline and modeling steps

The key data preparation and modeling steps are listed below:

1. Calculating returns. In statistical modeling, it is customary to transform the times series data to make its distribution stationary. Transformation for interest rate time series usually involves calculating daily differences or absolute returns ²⁵.

$$x_t = R_t - R_{t-1} \quad (41)$$

Transformation for stock prices usually involves calculating relative returns or log returns.

$$x_t = \log(P_t) - \log(P_{t-1}) \quad (42)$$

To differentiate the original time series and its returns, the original time series is usually referred to as “levels”.

For the 9-tenor USD Libor curve (USDYC1) dataset, from 12/31/2007 to 2/25/2022, there are 3550 business dates, and the returns (rate change) dataset has 3549 business dates (1/2/2008-2/25/2022). The returns array x is 3549×9 .

2. Standardization or normalization. To improve model fitting, the data are usually standardized (transformed to mean zero and standard deviation 1.0) or normalized (usually to a range of $[0, 1]$ or $[-1, 1]$). For image data, all pixel values are in the range $[0, 255]$, normalization to a standard range is preferred. For random financial data such as yield curve, standardization to zero mean and unit variance is used to scale the returns. The scaled data are used in model fitting. After synthetic data are generated, they are “unscaled” to the original form for comparison with the raw returns data.

Note that activation function used in neural networks needs to be consistent with the range of values expected. For example, if the output range from the network is expected to be $(-\infty, +\infty)$, then an activation function that restricts the output range to be in the range $[0, 1]$ is inappropriate. For this reason, linear activation for the final layer in the generator is used in this paper.

For USDYC1, the standardized returns array x is 3549×9 .

3. Windowing, time slicing or sequencing. Imaging application is an important use case for the development of deep learning models and helps to shape the deep learning models for later applications. For an application, the image size is usually fixed. For example, images in the well known MNIST ²⁶ image dataset are of fixed size 28×28 . The setup of

²⁵There is a long standing debate on whether interest rates follow a normal or lognormal model. A normal model would imply that absolute return is appropriate, while a lognormal model would imply that log-return is appropriate. In this paper, we follow the intuitive normal model and use absolute returns.

²⁶See <http://yann.lecun.com/exdb/mnist/>.

neural network for financial time series follows image application. Since deep learning models usually expect a dataframe or sequence of a fixed size, time series data in 2-dimensional arrays are sliced into time windows of fixed size. For a typical model in the paper, the 9-tenor USD yield curve²⁷ is sliced (or windowed/sequenced) into windows of 20 business dates. Each sequence is a 2-dimensional array (of dimension 20×9), which is similar to an image in deep learning models for imaging applications. This is called sliding or rolling windows (of length 20) in statistical modeling. Concatenating all sequences to an array forms a 3-dimensional array, which are used in model fitting. The first 10 days in the sequence are used as condition and the second 10 days in the window are used as target for prediction (or “label” for supervised learning). The 3-dimensional array is similar to a collection of images. Each 2-dimensional array (20×9) is called a dataframe, a window, a slice or a sequence. In general, a sequence is of dimension $(p+q) \times d$, with p the condition length, q the target sequence length, and d the number of time series (features). For USD yield curve application in this study, $p = 10, q = 10, d = 9$. For USDYC1, the sequenced 3d array is $3530 \times 20 \times 9$.

4. Train-test (or train-validation) split. The windowed data are split into train-test datasets randomly (in the window dimension or the first dimension of the 3d array), with 80% in train and 20% in test.

For USDYC1, there are 2824 rows in the train data and 608 rows in the test data. In another word, there are 608 test dates in the test data.

5. Model fitting (training). The model is trained (fitted) on the train dataset.

6. Model validation:

- (a) Synthetic data generation. For each sequence in test dataset, synthetic data are generated. For example, a test sequence includes data for 20 business dates from 12/13/2021 to 1/11/2022²⁸. The 10-day data from 12/13/2021 to 12/27/2021 are used as condition to generate synthetic data for the 10-day period 12/28/2021 to 1/11/2022. The synthetic data can be compared with the test data for the same period (12/28/2021 to 1/11/2022). This test sequence is used to generate forecast for 10 days after business date 12/27/2021. For simplicity, we can say that for this test sequence, the test date is 12/27/2021. This is analogous VaR calculation: suppose the current date is t_0 (test date), we need to forecast the distribution for the next 10 dates $t_0 + 1, \dots, t_0 + 10$.

²⁷For any business date, there are nine interest rates for different maturities. An yield curve is defined as yield (interest rate) as a function of time to maturity or tenor.

²⁸The 20×9 20-day test data can be further divided into a 10×9 array for the first 10 days as test condition, and 10×9 array for the second 10 days as target data for validation.

When a large number of copies (or paths) of synthetic data are generated for each day in a period, the synthetic data form an empirical distribution for each date in the period. Test data can be compared with the synthetic data distribution on corresponding dates to assess the quality of the synthetic data distribution. This is done as part of backtesting KPI.

- (b) KPI calculation. KPIs are calculated by comparing test and synthetic data in statistical distribution and autocorrelation. The calculation of these KPIs uses the 20% data reserved for testing or validation. See Section 4.3 for details.
- (c) Backtest. Backtesting is an important part of model validation for VaR models and is usually implemented using data for consecutive dates. Furthermore, the 20% data in the test dataset (that covers non-consecutive dates) may not be enough for backtesting. For these two reasons (non-consecutive dates and not enough data), we perform backtesting using data on every eligible dates. This gives us more data points to assess the quality of the models. For this purpose, synthetic data need to be generated for every date, which is why the backtest step can be time consuming for some models. See Table 9 for the running time of the backtest step of each model. Because backtest uses data on every eligible dates, unlike other KPIs, backtest KPI is not strictly out of sample.
- (d) Combination of KPIs into a composite score. Distribution, autocorrelation and backtest KPIs are combined into a composite score. See Section 4.3.

Note that all KPIs are calculated using returns.

4 Performance comparison

In this section, we discuss details of model testing methodology and results. The computing platform for model testing is described in Section 4.1. Hyperparameter tuning is discussed in Section 4.2. As a result, a set of hyperparameter settings and list of model specifications forms the basis for model testing. KPIs for model comparison are discussed in Section 4.3. Model testing results using simulated data are presented in Section 4.4, and model results using historical data are presented in Section 4.5.

4.1 Computing platform

The computing platform for model testing is as follows: OS: Red Hat Enterprise Linux Server 7.9 (Maipo) fedora, Architecture: x86_64, Model name: Intel(R) Xeon(R) Gold 6138 CPU @ 2.00GHz, CPU(s): 80, GPU: NVidia V100-PCIE-32GB, Driver Version: 510.47.03, CUDA Driver Version: 11.6, RAM: 527GB.

We add the following notes on the coding for the study:

Table 9: Model running time (in minutes) for dataset USDYC1 (Libor curve)

No.	CAT	MODEL	TRAINING	GENERATION	BACKTEST	KPI	TOTAL
1	HS	FHS	0	0	0	7	7
2	HS	PHS	0	0	0	8	8
3	PM	AR	1	0	1	7	9
4	PM	AR-RET	1	0	1	7	9
5	PM	GARCH	7	0	1	7	15
6	PM	GARCH-RET	7	0	1	7	15
7	PM	GARCHt-RET	11	0	1	7	19
8	PM	NS-VS	0	0	1	7	8
9	NN	CGAN-FC	50	0	0	7	57
10	NN	CGAN-LSTM	109	0	1	7	117
11	NN	CWGAN	149	0	0	7	156
12	NN	DIFFUSION	28	10	21	7	66
13	NN	SIG	79	0	0	8	87
14	NN	VAE	0	0	1	7	8

- For several neural network models (Diffusion, SIG, VAE), the code from external github is used as the starting point, we then made improvements as needed. See Section A.1 for external githubs used.
- For CGANFC, CGANLSTM and CWGAN, we developed the code by ourselves.
- For HS and all parametric models, we developed the code by ourselves.

For all models, the code is factored so that model training and validation follow the same steps: data scaling, training, generation, backtesting and KPI calculation.

For typical parameter settings, the model running time ²⁹ in minutes for USDYC1 dataset is presented in Table 9. It can be observed that the top three time consuming models are CWGAN, Diffusion and LSTMCGAN. CWGAN and LSTM are slow in training and Diffusion model is slow in backtesting. To save time in backtesting step, the number of business dates in backtesting for Diffusion model are reduced from 3028 to 1216. As a result, the running time for backtesting step for Diffusion model is reduced from 61 minutes to 21 minutes for USDYC1 dataset. The two sets of backtest dates generate similar backtesting KPI. As a result, for extensive model testing, a reduced number of backtest dates is used for Diffusion model.

Relative to production grade models with millions or billions of parameters, the NN models in this study are very limited in scale (most of the NN networks have 3~5 layers only). This is also a reflection of the short time series for historical data used in the study.

²⁹The code does not track the running time for KPI calculation currently.

Hyperparameter	Note
Data processing	
dataset	Training dataset name
Input data return type	Return type of the input data (absolute or relative)
Train-test split percent	80% train and 20% test split in general
data split seed	Seed to split the data
Trainer	
batch size	Batch size of training data
epochs	Training total steps
condition length	Condition length
sequence length	Target sequence length for forecasting
scaler type	data transformation type (MinMaxScaler or StandardScaler)
activation function	Activation function
noise_dim	noise dimension
Generator	
generator.seed	Generator seed
n_synthetic	Number of copies of synthetic data to generate
long path steps	The long path steps for generator
short_path_steps	short sequence length of the generated data (for calculating KPI), normally same as training sequence length
long_path_steps	long sequence length of the generated data (for calculating ACF)
Common parameters	
optimizer	By each model
learning rate	controls how much to change the model in response to the estimated error each time the model weights are updated
Network parameters	
network type	By each model
layers	number of layers
clip value	The upper bound of clipping the weights in GAN
hidden_dim	hidden dimension of the network (often in latent space)

Table 10: Model configuration and hyperparameter list

4.2 Hyperparameter tuning

Model performance depends on hyperparameters that define network structure and training mechanics. Deep learning models have various hyperparameters, including model structural parameters, configuration parameters, as well as data preprocessing/postprocessing parameters. To ensure consistency across all models that are evaluated, the same configuration/hyperparameters are applied as much as possible. The following model configuration and hyperparameters are in the setup files that can be adjusted for each model run.

Our major efforts over hyperparameter tuning is on the trade-off between model stability and performance. Overall, we have tested different sequential length of sliced data to better align to the model use, and finally chose to set condition length to 10, and target sequential length to 10.

The following hyperparameters and variations are tested for applicable models:

- GAN: clipping value. Specifically on LSTM CGAN, clip_value 0.05, 0.075, 0.1, 0.75 are tested and 0.075 was chosen.
- VAE: weights on different loss function components are tested.
- Signature: different prediction model in signature space (predicting future signature from past signature). Linear, NN with dense layers, and NN with CNN layers are tested. NN with CNN layers are adopted. See the online appendix for details.
- Nelson-Siegel representation for yield curve: both AR+GARCH and Vasicek model are considered for the dynamics of the three factors. NS with Vasicek dynamics performs better and is adopted. See the online appendix for details.
- AR and Vasicek models ³⁰ : AR and Vasicek models are very close. Model testing shows that they have similar performance. The simpler AR model is used in model comparison. See the online appendix for details..

To be consistent across all models, we carefully designed network structure to enable apple-to-apple performance comparison. Despite the significant differences among all network structures embedded in the different model architectures, one of the common hyperparameters is the dimension of the random noise z as input ($noise_dim$). For a typical linear three factor model of the yield curve (e.g. Nelson-Siegel model), we replicate (13) below,

$$R_t(\tau) = b_{0t} + b_{1t}f_1(\tau) + b_{2t}f_2(\tau)$$

where $R_t(t)$ is yield for tenor τ at time t , $f_1(\tau)$ is loading of slope factor on tenor τ , and $f_2(\tau)$ is loading of curvature factor on tenor τ . $b_{it}, i = 0, 1, 2$ are random factors. With this three factor model for a nine tenor yield curve, three random numbers (b_{0t}, b_{1t}, b_{2t}) are used to generate nine yields.

For some models (CGAN, CWGAN, Diffusion, TimeVAE), $noise_dim$ is used to generate random noise for each condition/business date, which is in turn used to generate a 10×9 sequence for a typical model of generating daily 9 tenor yields for the next 10 days ($step = 10$), thus 90 yields.

- For USD yield curve, this parameter is set to $noise_dim = 30$, equivalent to a three factor model. In such cases, 30 random numbers are used to generate 90 yields, or equivalently, three random numbers are used to generate nine yields.

³⁰Strictly speaking, this is not hyperparameter selection, but this shows how the model selection decision is made.

- For simulated two tenor data, $noise_dim = 20$ is used, which is equivalent to a two factor (or full factor) model. A value lower than 20 would imply a model that may be too simple and restrictive.

For other models (LSTM and Signature), $noise_dim$ is used to generate random noise for each step (of 10 steps) in generation, thus $10 \times noise_dim$ random numbers are used to generate a 10×9 sequence for a typical model of generating daily 9 tenor yields for the next 10 days, thus 90 yields.

- For USD yield curve, this parameter is set to $noise_dim = 3$, equivalent to a three factor model.
- For simulated two tenor data, $noise_dim = 2$ is used, which is equivalent to a two factor (or full) model.

This study does not include comprehensive testing of hyperparameters.

For parametric models, AR models are estimated with 5-year window (252×5 dates), GARCH models are estimated with 3-year window (252×3 dates).

4.3 KPIs for model comparison

We quantify what it means for a set of generated synthetic samples to have similar statistical properties (“look like”) to the real data. Real data here refers to windowed historical data in the testing dataset, which is 20% of the available real data in a typical application. Details of the data preparation pipeline are discussed in Section 3.2.3. We generate both short-path (10 days) and long-path (502 days) synthetic samples from each generative model. Short-path synthetic samples use the single-step prediction method. Long-path synthetic samples use the iterative method to generate multi-step prediction of 502 days. See Section 2.4 for details. Only the ACF plot (Figures 6 and 13) uses long-path synthetic samples. All other plots and metrics use short-path synthetic samples.

Table 11 provides a list of qualitative and quantitative measures we use to compare the performance of different models.

We examine the fidelity of synthetic data to the real data using qualitative and quantitative measures. Qualitative measures include empirical distribution visual comparison, t-SNE, PCA and UMAP. Quantitative measures include distribution distance (Earth Moving Distance, DY and KS distance metrics, Series distance), ACF and backtesting. Details are described below.

Model rankings vary depending on the KPIs used and the way they are combined to form the composite score.

4.3.1 Qualitative measure

We visualize the distribution of real versus generated distributions with and without log scale. Figure 6 shows an example visualization of histograms and ACF plots. Real data in the plots

Table 11: List of measures for model comparison

KPI Category	Measure
Distribution	Distribution and ACF plots
	Distribution distance (DY)
	Earth moving distance (EMD)
	*Kolmogorov-Smirnov test (KS) of sample moments
	Series distance
	*Kolmogorov-Smirnov test (KS) of returns
Correlation	Inter-tenor correlation matrix
	ACF score
	*Fisher test of equality of correlation
Embedding	t-SNE
	UMAP
	PCA
Backtesting	u-value histogram
	u-value histogram ranges
	u-value histogram difference from 1.0
	u-value breach rate (diff from theoretical) from 1.0
	Envelope plot
	*Kolmogorov-Smirnov test (KS) of u-values
Combination of KPIs	KS of moments + KS of returns → Distribution (DIST) score
	Breach rates + KS of u-value → Backtest (BT) score
	Distribution + ACF (Fisher test) + BT → Composite score

(Only a subset (*) of KPIs are combined to form Composite score.)

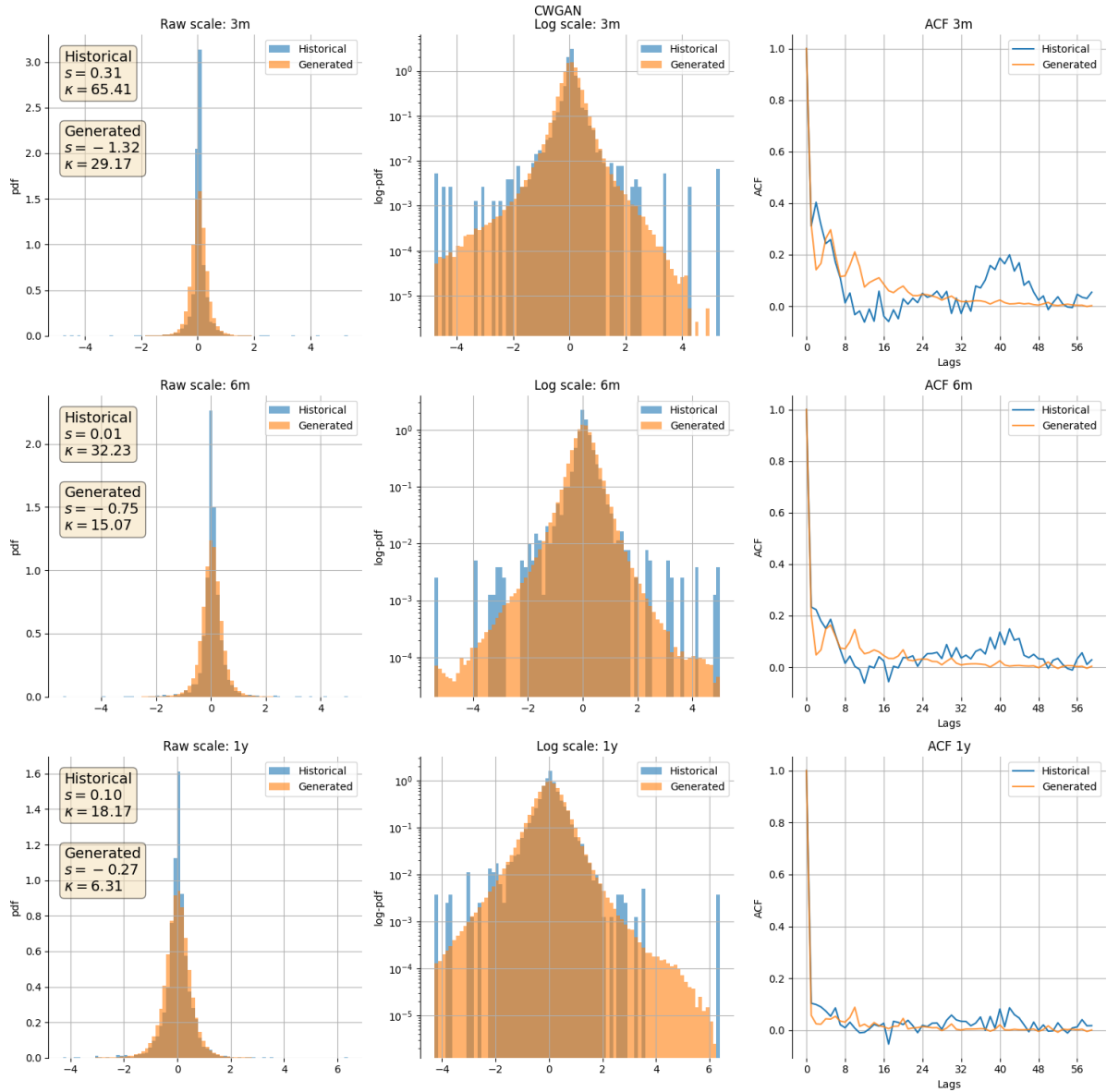


Figure 6: Example of empirical distribution visualization

is test samples of windowed historical data. For synthetic data, the histogram uses short-path synthetic samples, while ACF plot uses long-path synthetic samples to cover longer lags.

We use three dimensionality reduction techniques to map real data and synthetic samples onto a two-dimensional space and compare their distributions. These are visualizations, hence, qualitative measures.

Empirical distribution and ACF plot

Examples of empirical distribution of test and synthetic data and ACF are presented in Figure 6. It shows visual comparison of distributions and ACF.

PCA

Principal component analysis (PCA) is a statistical technique that performs linear dimensionality reduction for a dataset. This is accomplished by linearly transforming the data into a new

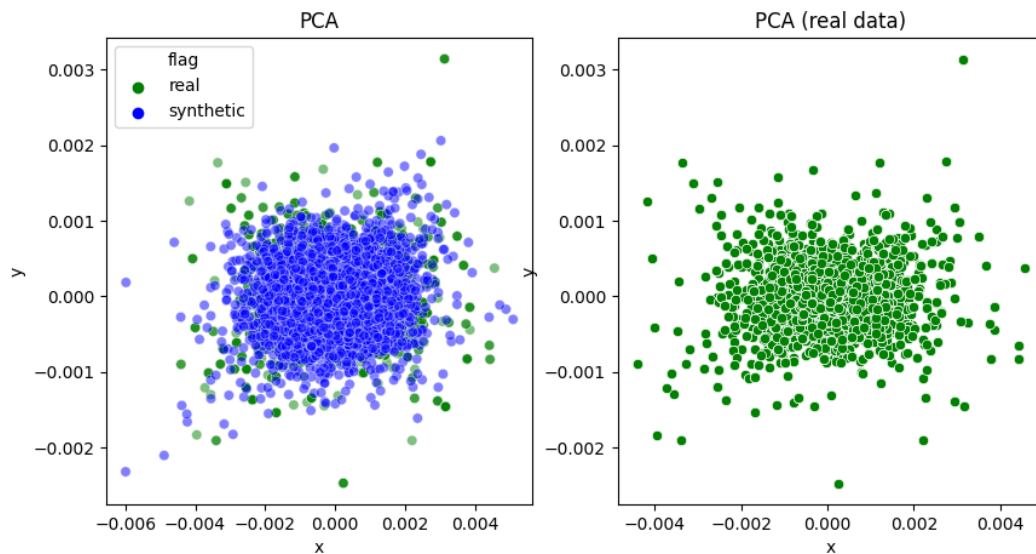


Figure 7: Example of PCA visualization

coordinate system where (most of) the variation in the data can be described with fewer dimensions than the initial data. Many studies use the first two or three principal components, and plot the data in two dimensions and to visually identify clusters of closely related data points.

We use PCA to project real and synthetic data onto two-dimensional space for visualization. Figure 7 shows an example of PCA results. Real data and synthetic data also covers similar regions in the projection space ³¹.

t-SNE

t-SNE (t-distributed stochastic neighbor embedding) is introduced in 2008 in [van der Maaten and Hinton \(2008\)](#). It is a non-linear method that maps high-dimensional data into a low-dimensional space, while preserving the pairwise similarities between data points. The mathematics of t-SNE involves two main steps. First, t-SNE constructs a probability distribution over data points in high-dimensional space using a Gaussian kernel. Second, t-SNE defines a similar probability distribution over the points in the low-dimensional space, and it minimizes the Kullback–Leibler divergence (KL divergence) between the two distributions. Compared with PCA, t-SNE can be characterized as a nonlinear dimensionality reduction technique ³².

Figure 8 shows an example t-SNE visualization. Figure on the left shows the data points for real data and synthetic data together, while the figure on the right shows only the points from the real data. We can see the synthetic data covers similar regions as the real data.

UMAP

³¹Two plots are shown because real and synthetic data often show a high degree of overlap and it is hard to tell whether real data are covered by (a subset) or overlapped with synthetic data.

³²For a comparison of PCA and t-SNE, see <https://www.geeksforgeeks.org/difference-between-pca-vs-t-sne/>

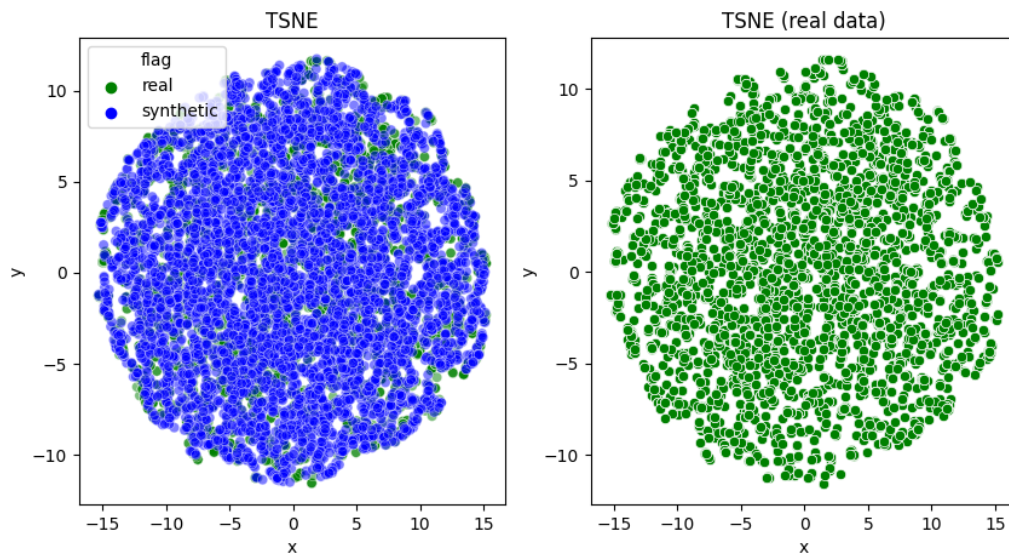


Figure 8: Example t-SNE visualization

UMAP (Uniform Manifold Approximation and Projection) was proposed in 2018 in [McInnes et al. \(2020\)](#). It constructs a topological representation of the high-dimensional data and then projects it onto a lower-dimensional space. This is done by constructing a weighted graph of the data, where vertices represent the data points and the edges represent the relationships between the points. UMAP is effective in preserving both global and local structure in high-dimensional data ³³.

t-SNE and UMAP are related and different as follows ³⁴: t-SNE uses a Gaussian probability function to calculate how likely a cell will pick another cell as its neighbor, and repeats this step for all cells. In the low dimension space, cells are rearranged according to these distances, creating the t-SNE plot. UMAP, in a more clever way, creates a fuzzy graph that accurately reflects the topology (a.k.a shape) of the true high dimensional graph, calculates the weight for edges of this graph, then builds the low dimensional graph mimicking the fuzzy graph. In another word: while t-SNE moves the graph point-to-point from high to low dimensional space, UMAP makes a fuzzy, but topologically similar graph and compresses it into a lower dimension.

We apply UMAP to map the real and synthetic data onto two-dimensional space. Figure 9 shows an example of UMAP visualization. synthetic data cover similar regions as the real data in 2D space.

³³For a detailed description of UMAP, see <https://umap-learn.readthedocs.io/en/latest/>

³⁴For more details, see <https://blog.bioturing.com/2022/01/14/umap-vs-t-sne-single-cell-rna-seq-data-visualization/>.

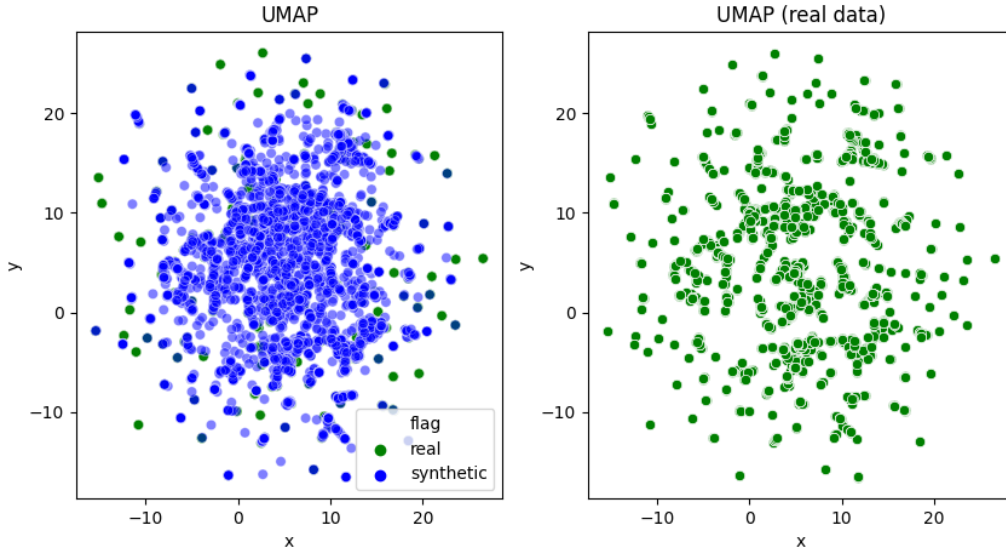


Figure 9: Example UMAP visualization

4.3.2 Distribution comparison

For each test date t , one copy of the windowed return \tilde{x}_t is generated, and this is a $q \times d$ array (typically $q = 10$, $d = 9$ for yield curve). Sample moments (mean, standard deviation, skewness and kurtosis) for each \tilde{x}_t (in the q dimension) is calculated. This is calculated for each test date for real data x_t and synthetic data \tilde{x}_t , producing a set of sample moments. Take the sample mean for example. Suppose there are S test dates in total, this procedure creates an array of size $S \times d$ sample means for the real data, and an array of size $S \times d$ sample means for synthetic data. The distribution of the sample mean across all S test dates are presented in Figure 10.

Sample means of the synthetic data and sample means of real data are tested for whether they are from the same distribution. Other sample statistics (standard deviation, skewness and kurtosis) can also be used in the testing. However, since the typical sequence length is $q = 10$ days, skewness and kurtosis calculated from 10 data points may not be reliable. Therefore, only sample mean and sample standard deviation are used in the testing.

The sample moments are used to calculate distribution distance in Section 4.3.2.1. The returns are used to calculate series distance in Section 4.3.2.2.

4.3.2.1 Distribution distance We measure distribution distance using EMD, DY and KS metrics. Details are provided below.

Earth Mover or Wasserstein-1 distance (EMD) Let \mathbb{P}_r denote the historical distribution $X \sim \mathbb{P}_r$, and \mathbb{P}_g the generated distribution $\tilde{X} \sim \mathbb{P}_g$. Let $\prod(\mathbb{P}_r, \mathbb{P}_g)$ denote the set of all joint probability distributions with marginals \mathbb{P}_r and \mathbb{P}_g . The earth mover distance (Villani (2008)) describes how much probability mass has to be moved to transform \mathbb{P}_r into \mathbb{P}_g . Details of EMD are discussed in Villani (2008).

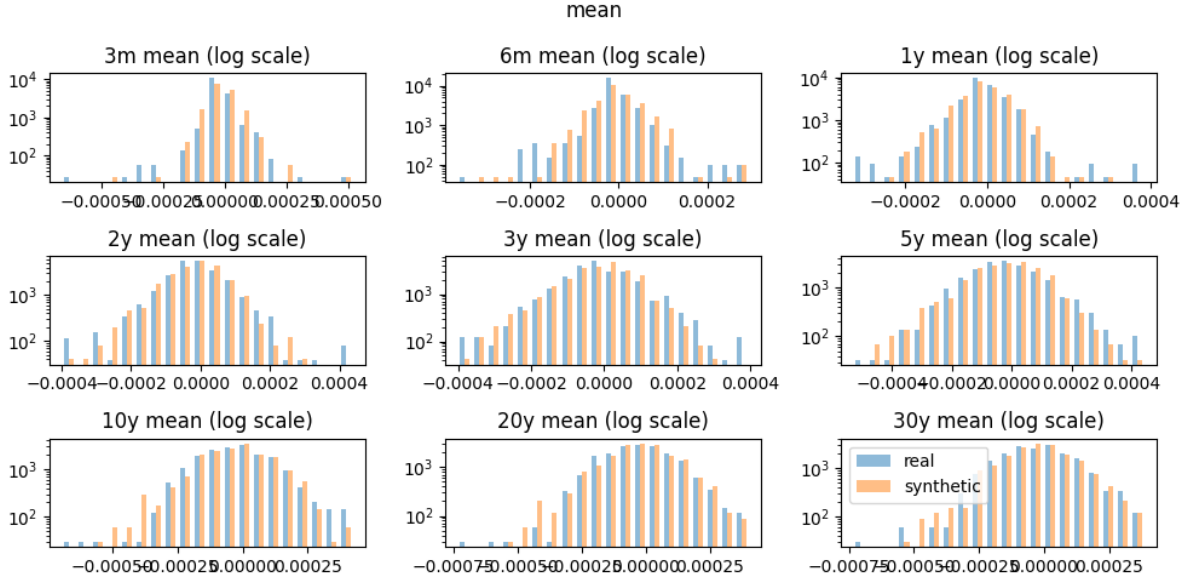


Figure 10: Example of histogram of sample mean

EMD is defined by:

$$\text{EMD}(\mathbb{P}_r, \mathbb{P}_g) = \inf_{\pi \in \Pi(\mathbb{P}_r, \mathbb{P}_g)} E_{(X, \tilde{X}) \sim \pi} (\|X - \tilde{X}\|) \quad (43)$$

This is the infimum across all joint distributions. It is shown Ramdas et al. (2015) that EMD can be calculated as the following ordinary integral (without the infimum)³⁵ :

$$\text{EMD} = \int_{-\infty}^{\infty} |F_X(s) - F_{\tilde{X}}(s)| ds \quad (44)$$

where F_X and $F_{\tilde{X}}$ are the CDF of random variables X and \tilde{X} respectively.

Distributional metric: DY metric

DY metric is proposed in (Dragulescu and Yakovenko (2002)). The DY metric is defined by:

$$DY = \sum_x |\log P_r(A_x) - \log P_g(A_x)| \quad (45)$$

where P_r and P_g denote the empirical probability density function of the historical and generated path. Further, (A_x) denotes a partitioning of the real number line such that for all x we (approximately) have $\log P_r(A_x) = \frac{5}{T}$ for T the number of historical returns.

KS distance

The Kolmogorov-Smirnov (KS) distance measures the similarity between the empirical CDF of real data and synthetic samples. It is the max absolute difference of the empirical pdf.

³⁵See https://docs.scipy.org/doc/scipy-1.7.1/reference/generated/scipy.stats.wasserstein_distance.html

Table 12: Example distribution distance for dataset USDYC1 (Libor Curve)

Statistic	Tenor	EMD	DY	KS	KS_{pval}	$1 - KS_{pval}$
mean	3m	0.013	1.289	0.252	0.000	1.000
mean	6m	0.012	1.095	0.191	0.000	1.000
mean	1y	0.009	0.964	0.118	0.000	1.000
mean	2y	0.008	0.896	0.035	0.862	0.138
mean	3y	0.009	0.846	0.043	0.635	0.365

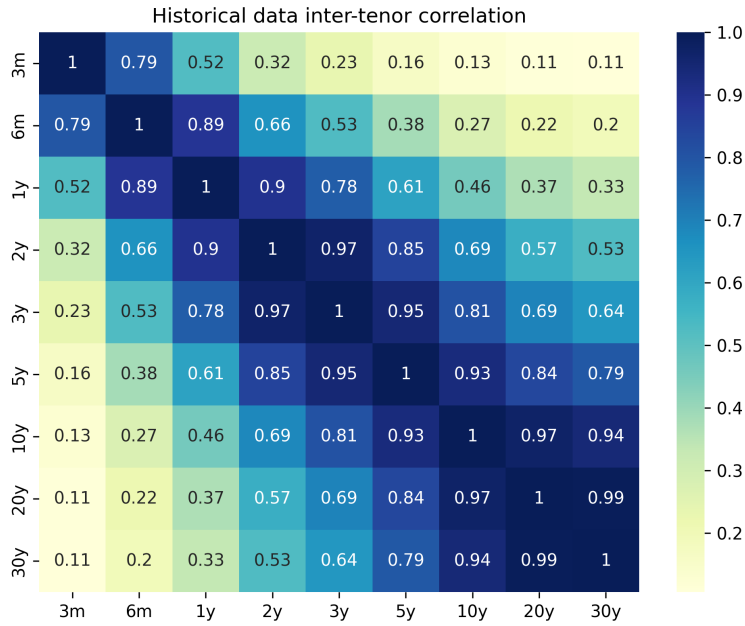


Figure 11: Example of historical data returns correlation matrix

Sample result for distribution distance is presented in Table 12. In the table, KS_{pval} is the p value (significance level) of the two-sample KS test. $1 - KS_{pval}$ is 1 minus KS_{pval} , which is used in model ranking since a smaller value of $1 - KS_{pval}$ (a larger value of KS_{pval}) indicates a better model.

4.3.2.2 Series distance In model comparison, for simplicity, the two-sample KS test for distribution is used for series distance. It is calculated using the returns rather than the sample moment of returns.

4.3.3 Inter-tenor correlations

We estimate the cross tenor covariance and correlation of real and synthetic returns. Figure 11 shows an example of cross tenor correlation matrix for USDYC1 dataset. Figure 12 shows the difference between correlation matrices of real and synthetic data.

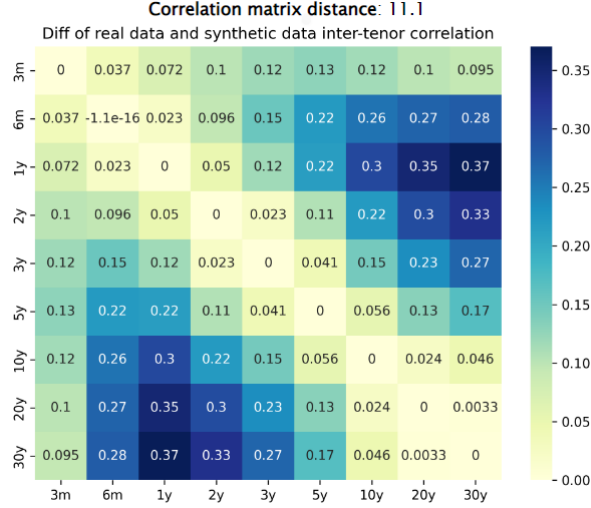


Figure 12: Example of correlation matrix distance visualization

4.3.4 Autocorrelation

It is straightforward to calculate autocorrelation (ACF) for a time series x_t . Let the ACF with lag l be denoted as,

$$C(l; x) = \text{Corr}(x_{t+l}, x_t)$$

However we need to go through some tricky steps because the real and synthetic data are in sequence form (3-dimensional array) rather than in time series form (2-dimensional array). For discussion, let X be a 3-dimensional array, with the first dimension for test date or sequence number, the second dimension the sequence length $q = 10$, and the third dimension $d = 9$ for tenor. ACF should be calculated along the second dimension $q = 10$ (for dates $t + 1, \dots, t + q$). However, since the length of the time series (time dimension) is only 10, there isn't enough data to calculate ACF for longer lags. For illustration, we select one tenor and fix the resulting 2D array $X = (x_{ij}), i = 1, 2, \dots, N, j = 1, 2, \dots, q$ array. Prior to model training, the whole dataset is split randomly into train and test datasets. As a result, the test date that the first dimension of X represents, t_i , is not even consecutive, highlighting the fact that ACF is calculated along the second dimension of X . To increase the sample size for ACF calculation, we form all pairs of a given lag from all sequences. For fixed i , lag 1 pairs can be formed from $(X(i, j), X(i, j+1)), j \leq q - 1$, only 9 pairs for $q = 10$. This is hardly enough to calculate the first order ACF. The trick is to let i vary and we collect all lag 1 pairs from all sequences. Hypothetically, if there are 600 sequences of length 10, this procedure forms a sample of lag 1 pairs of size $600 \times 9 = 5400$, much more data than just 9 observations for first order ACF calculation in one sequence.

For any function f , ACF can also be calculated for $f(x)$. For financial time series, $f(x) = |x|$ and $f(x) = x^2$ is particularly relevant since the ACF for these $f(x)$ captures volatility (or variance) clustering. Figure 13 shows an example visualization of real versus synthetic

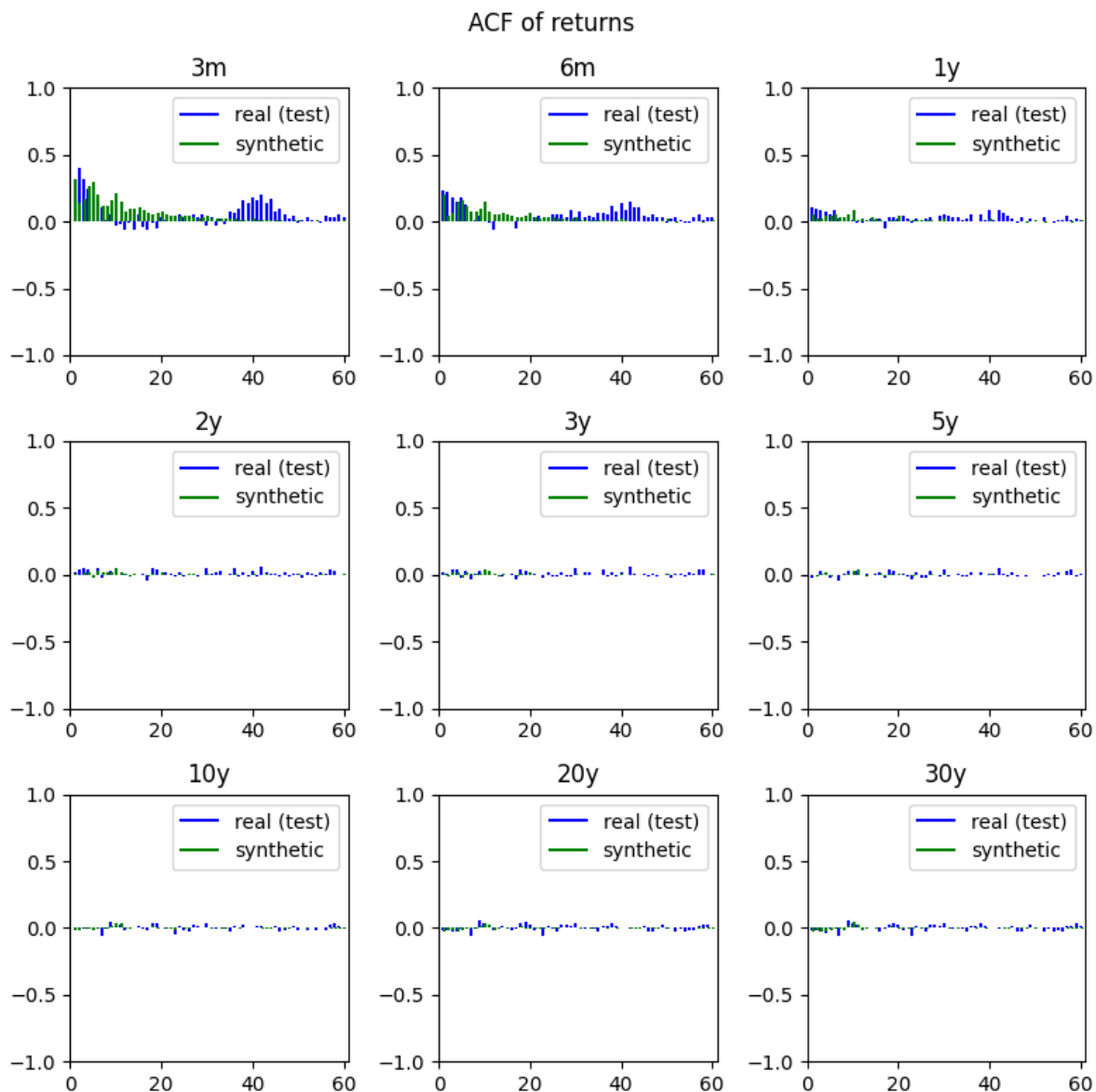


Figure 13: Example visualization of real versus synthetic autocorrelation for returns

autocorrelation for $f(x) = x$, and Figure 14 for $f(x) = x^2$ ³⁶. It can be observed that the ACF for squared returns (Figure 14) is much stronger than the ACF for returns (Figure 13), which is typical of financial time series.

The **ACF score** $ACF(f)$ is a summary measure of the ACF difference for several lags. Let $C(x)$ be a vector of ACF at several lags (since $q = 10$, ACF at only lags 1 and 2 are calculated),

$$C(x) = (C(1, x), C(2, x))$$

The ACF norm score is just the L_2 norm of the difference of the ACF vector of real and synthetic

³⁶In addition to the regular ACF, leverage ACF can also be calculated, leverage ACF = $Corr(x_{t+1}^2, x_t)$, which measures the correlation of variance with lagged returns (the leverage effect). For financial time series, volatility clustering is a much stronger feature than the leverage effect.

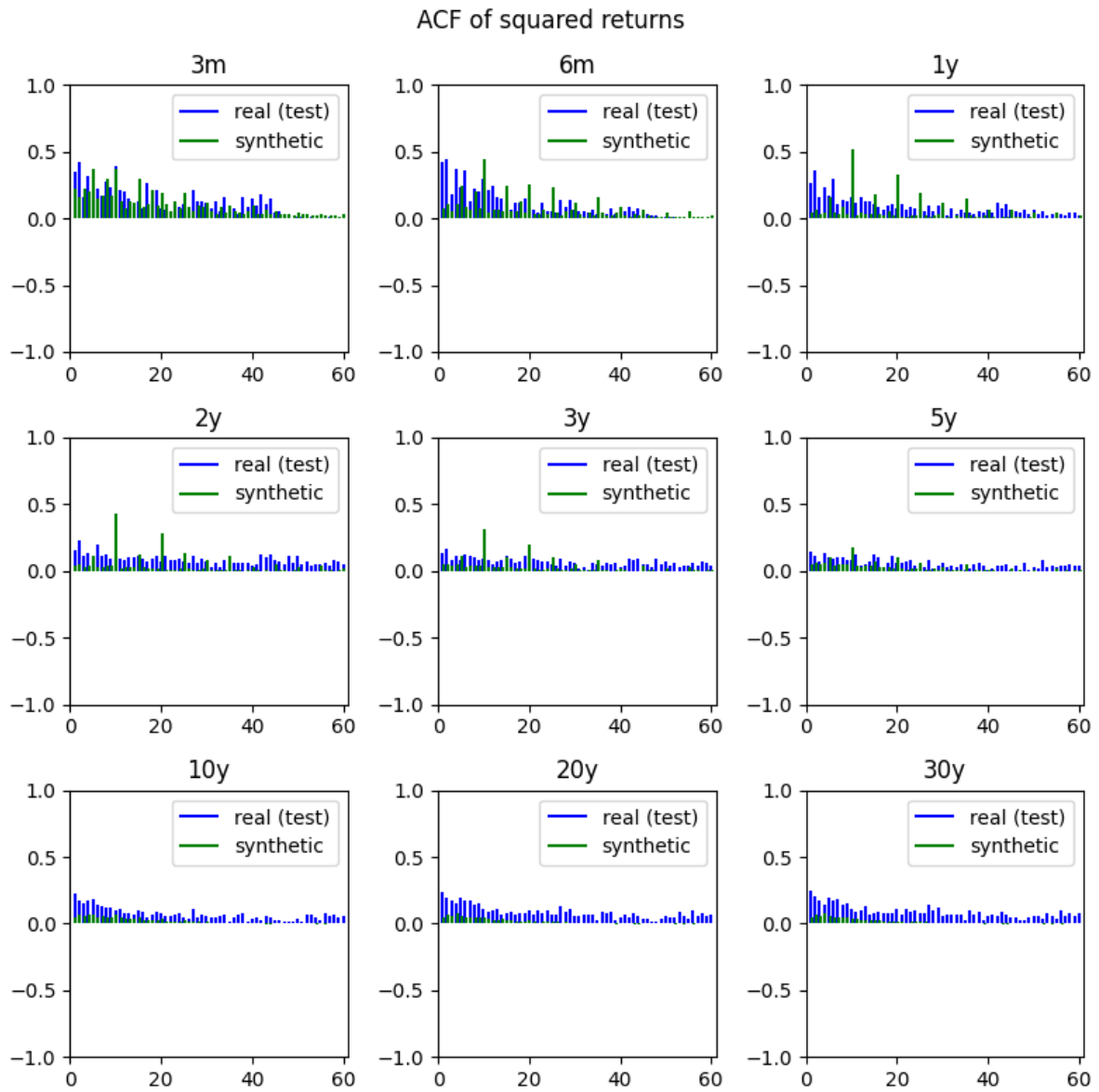


Figure 14: Example visualization of real versus synthetic autocorrelation for returns squared

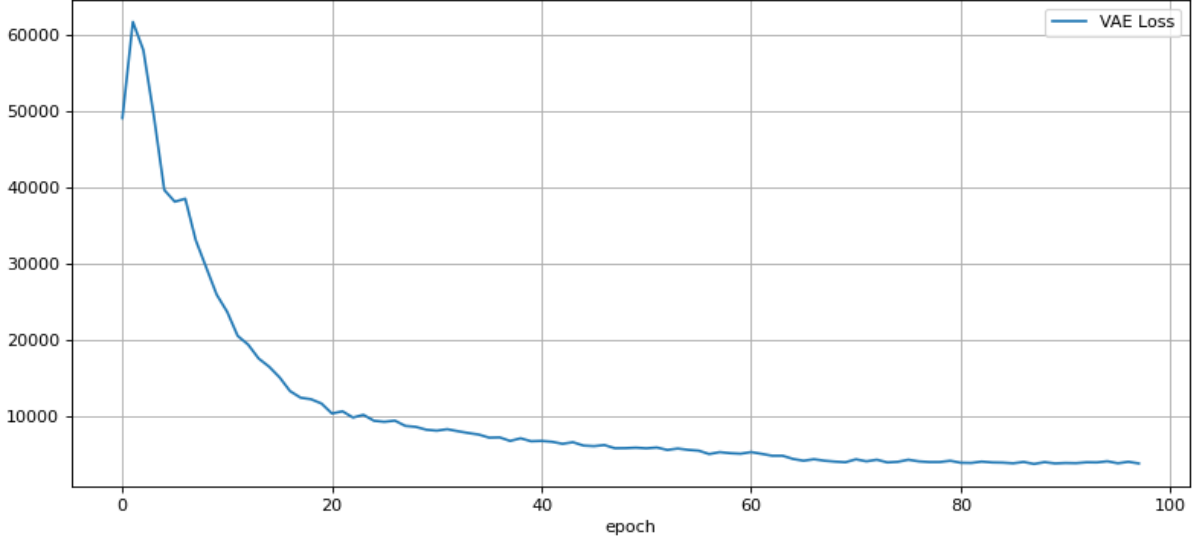


Figure 15: Example loss function visualization

data.

$$\text{ACF}(f) = \left\| C(f(x)) - C(f(\tilde{x})) \right\|_2$$

where the function f is applied element-wise to the series. The ACF norm score is computed for the functions $f(x) = x$, $f(x) = |x|$ and $f(x) = x^2$.

To facilitate the calculation of a composite score later, the comparison of ACF (for any pair of correlation coefficients ρ_1 and ρ_2) is converted into probability space using the Fisher Z-transformation³⁷. This ACF score is defined as,

$$\text{ACF}(\rho_1, \rho_2) = 1 - \Phi \left(\frac{|\rho_1 - \rho_2|}{\sqrt{\frac{1}{n_1-3} + \frac{1}{n_2-3}}} \right) \quad (46)$$

where Φ is the CDF of a standard normal distribution, and n_i are the number of observations used to calculate ρ_i .

For ACF vectors, $C(x)$ (for real data) and $C(\tilde{x})$ (for synthetic data), a vector $\text{ACF}(\rho_1, \rho_2)$ is calculated using the Fisher Z-transformation. $\text{ACF}(\rho_1, \rho_2)$, $\rho_1 \in C(x)$, $\rho_2 \in C(\tilde{x})$ is used in the calculation of the composite score.

4.3.5 Training loss

We visualize the loss function over training epochs to evaluate convergence of the model. Figure 15 gives an example of the loss function for VAE model.

³⁷See <https://github.com/psinger/CorrelationStats/blob/master/corrstats.py>.

4.3.6 Backtesting

Backtesting is a common requirement to assess the quality of VaR models ³⁸.

In probability theory, the probability integral transform³⁹ (PIT) states that, for any random variable X with a continuous distribution and cumulative density function (CDF) $F(x)$, the random variable $Y = F(X)$ follows a uniform distribution. Let X_i be a series of random variables with CDF $F_i(x)$, and $x_i \sim F_i, i = 1, \dots, N$ be a random sample, then, $y_i = F(x_i), i = 1, \dots, N$ is an independent sample from the uniform distribution. Note that each x_i is sampled from its own true distribution. A statistical test for $\{y_i\} \sim U[0, 1]$ is equivalent to the joint test $x_i \sim F_i(x), i = 1, \dots, N$. This idea has been used in the context of backtesting market risk VaR models. See Crnkovic and Drachman (1996); Berkowitz (2001).

In our application, for each business date t , there is a condition $(x_{t-p}, x_{t-p+1}, \dots, x_{t-1})$ used to generate synthetic data for a range of dates in the future $\hat{x}_t, \hat{x}_{t+1}, \dots, \hat{x}_{t+q-1}$. We focus on x_t and \hat{x}_t (one step ahead generation). When N independent copies of \hat{x}_t are generated, which is denoted as $\hat{x}_t^j, j = 1, \dots, N$, it forms a distribution forecast \hat{F}_t for x_t . Let $y_t = \hat{F}_t(x_t)$, which is the probability value calculated for the actual data point x_t relative to the distribution forecast \hat{F}_t . Collecting y_t for multiple business dates, then the random sample $y_j, j = t, t + 1, \dots, t + N - 1$ follows uniform distribution under the assumptions that (1) x_j is independent for $j = t, t + 1, \dots, t + N - 1$, and (2) \hat{F}_j is the true distribution for $x_j, j = t, t + 1, \dots, t + N - 1$. y_t is called u-value instead of p-value for two reasons, (a) y_t follows a uniform distribution under the null hypothesis of correct model, (b) this distinguishes the p-value from a statistical test.

The uniformity of y_j can be assessed using different statistical tests, and the most well known test is the one sample Kolmogorov–Smirnov test (KS test). As with all statistical tests, the result of the KS test includes the value of the test statistic and the p-value of the test statistic in the null distribution. However, the independence assumption for the KS test may not hold, and the p-value of the KS test is only approximate.

We also use two intuitive metrics to measure deviation from uniformity. Create a histogram of u-values $y_j, j = t, t + 1, \dots, t + N - 1$ with 10 equal bins on the unit interval $[0, 1]$. Under uniformity, all bars in the histogram are of the same height. This has three implications, (1) the standard deviation among the height of the 10 bars is zero; (2) the range of the bars (the difference between the tallest bar and the shortest bar) is zero; (3) the deviation of the height of bars from 1.0 is zero. Therefore, the standard deviation, range of the u-value histogram bars, and deviation of the bars from 1.0 are the three intuitive measures we can use as indications of deviation from uniformity: the smaller, the closer to uniformity by each measure, and the better quality of the model producing the distribution forecast \hat{F}_j .

For market risk VaR model, a breach of the VaR model occurs when the realized loss of a trade or portfolio is greater than the VaR forecast at a confidence level for the day. For example, if the VaR forecast for the day is \$100 million, but the realized loss is \$105 million, then the VaR

³⁸For the online version, see <https://www.bis.org/bcbs/publ/d457.htm>.

³⁹https://en.wikipedia.org/wiki/Probability_integral_transform

Table 13: Sample backtesting scores for model CWGAN dataset USDYC1 (Libor curve)

J	DAYS	START	END	TENOR	KSpval	DIFF	BR05	BR95
1	1	2010-01-15	2012-01-17	3m	0.000	0.428	0.022	0.042
2	1	2012-01-18	2014-01-10	3m	0.000	0.909	0.004	0.006
3	1	2014-01-13	2016-01-08	3m	0.000	0.829	0.002	0.016
1	10	2010-01-15	2012-01-17	3m	0.000	0.405	0.028	0.038
2	10	2012-01-18	2014-01-10	3m	0.000	0.934	0.000	0.000
3	10	2014-01-13	2016-01-08	3m	0.000	0.925	0.000	0.028

is breached. A correct 99% VaR is expected to be breached with 1% probability. In a sample, a breach proportion (or rate) that is different from 1% is evidence of violation of the VaR model. This holds similarly for other breaching probabilities (e.g. 2.5%, 5%, 10% in the left tail and 90%, 95% and 97.5% in the right tail). For a small probability value, e.g. $p = 0.5\%$, breach rate in the left tail is counted, while for a large probability level, e.g. $p = 95\%$, breach rate in the right tail is counted. For use of backtesting with breach numbers in regulatory capital calculation for market risk, see [Basel Committee on Banking Supervision \(2019\)](#)⁴⁰.

A larger number of metrics are generated in backtesting, including (absolute) deviations from theoretical breach rates at 2.5%, 5%, 10%, 90%, 95%, 97.5%, (absolute) deviation of height of u-value histogram bar from 1.0, KS distance of u-value from uniform distribution. An example of various backtest scores is presented in Table 13. KSpval in the table is the p-value from KS test of u-values following a uniform distribution. "DIFF" in the table is the average absolute difference between the height of u-value histogram from 1.0.

To save space, the breach rate for only 5% (BR05) and 95% (BR95) are included. In the actual calculation, 2.5%, 5%, 10% in the left tail and 90%, 95% and 97.5% in the right tail are used. For each probability level p , BRp indicates the absolute difference between the actual breach rate and expected breach rate.

In the table, KSpval=0 for all six rows shown, indicating that uniform distribution of u-values for these sample periods and 3m tenor are rejected. DIFF column shows that the histogram is very different from uniform.

4.3.7 Combination of KPIs

We evaluate the performance of each generative model using multiple KPIs discussed in previous sections. Each KPI is calculated across multiple tenors and scores. To reduce the number of KPIs and make it easier for comparison, we combine KPIs across tenors and across score categories (or subscores).

Ideally, the KPIs can be combined through a statistically sound multivariate distribution. Given the diverse variety of KPIs considered, it is not intuitive how to do it. In this study, only KPIs in probability space (e.g. p-values from KS tests, p-values from Fisher's Z-transformation

⁴⁰For the online version, see <https://www.bis.org/bcbs/publ/d457.htm>.

and VaR breach rates) are combined through mean and median across tenors and KPI categories. It is somewhat ad hoc and arbitrary. We will continue to explore better ways to combine the KPIs.

Backtest

u-value analysis and backtest is performed across multiple tenors and sub-periods for 1-day and 10-day returns. Eight backtest scores are calculated. See 4.3.6 for details. The summary backtest score is calculated with the following steps,

1. Calculate eight backtest scores for each tenor and each 2-year sub-period (as well as whole period): $KSpval$, $DIFF$, $BR025$, $BR05$, $BR10$, $BR90$, $BR95$, $BR975$ (BRp is the absolute difference between the actual and theoretical u-value breach rate at probability level $p = 0.025, 0.05, 0.10, 0.90, 0.95, 0.975$). The sub-period analysis is intended to address the case in which a model performs badly in sub-periods (e.g. over- or under-estimate risk), but the problems in sub-periods when combined in the whole period and lead to good performance.
2. Calculate the median of each score across sub-periods.
3. Calculate the average between 1-day and 10-day scores.
4. Calculate the median across tenors.
5. Sum up breach rates at all six probabilities, $BR = BR025 + BR05 + BR10 + BR90 + BR95 + BR975$.
6. Calculate the sum, $BT = [BR + (1 - KSpval)]/2$. $1 - KSpval$ is used in the sum, since a smaller value indicates a better model, which is consistent with the breach rate BR .

$DIFF$ is excluded in the calculation of the summary backtesting score BT , since $DIFF$ itself is not a probability.

Distribution Distance Scores

Distribution distance (EMD, DY, KS, $1 - KSpval$) of 1-day returns using sample moments (mean and standard deviation) is calculated. $KSpval$ is the pval from KS test. $1 - KSpval$ is used since a small value of this metric indicates a better model. The summary score (DistributionDistance) is using only $1 - KSpval$, and is the average of scores across sample statistics (mean and standard deviation) and tenors.

Series Distance

Series distance is calculated as $1 - KSpval$, where $KSpval$ is the p-value from two sample KS test. Summary series distance is calculated as the average across tenors and between 1-day and 10-day scores.

ACF Score

To compare the autocorrelations in real and synthetic data, we calculate p-value (“ACF score”)

from Fisher's Z-transformation (46), for $f(x) = x$ and $f(x) = x^2$ separately. ⁴¹ . ACF score is further aggregated first by averaging ACF scores for x and x^2 , and then by averaging across all tenors. In model comparison, $1 - \text{ACF}$ is reported and used, since a smaller value of $1 - \text{ACF}$ indicates a better model, consistent with other KPIs.

Composite score

Multiple scores from different categories are combined further as follows. (1) The average of Distribution Distance (1-KS-pval from KS test for sample moments) and Series Distance ((1-KS-pval) from KS test for returns) is called Distribution (DIST) score, (2) The sum of Distribution (DIST) score, ACF score, and backtesting score (BT) is called Composite score (COMP). For all KPIs including Composite score, a smaller value indicates a better model. For an example of the combined score and model ranking, see Table 14.

Model rankings vary depending on the KPIs used and the way they are combined to form Composite score.

4.4 Results using simulated data

Daily data for 30 years are simulated following GARCH model and CIR square root model. Returns (rate changes) are simulated from GARCH model, and then accumulated over time to get level of rates. Rate levels are simulated from CIR model and returns are calculated as the daily change. These simulation models are called data generating process (DGP). See Section 3.2.

Each path from the simulation covers 30 years of daily data. All applicable models are run for each path. Since Nelson-Siegel is a term structure model for multiple tenors, it is not included in the model test for simulated dataset with bivariate time series. For each simulation model, five paths are generated and used in model testing. The 13 models are applied to the simulated levels or returns as appropriate. The model testing results are presented in this section.

There are several sets of tables for each DGP: (1) KPI and model ranking for one simulation path, Table 15. (2) Model ranking across all five simulation paths, Table 16. The ranking is done for each path individually. (3) The average KPI subscore (distribution, autocorrelation and backtest) across five datasets, Table 17. This shows, on average across five paths, how each model performs in each KPI category (or subscore). (4) The ranking by average subscore, Table 18.

More detailed results are available in an extended appendix (available upon request).

4.4.1 Results using simulated GARCH-normal Dataset

Each time series follows AR(1) model for its conditional mean and follows GARCH(1,1) model for its conditional variance. The conditional distribution follows normal distribution. See Section 3.2 for details.

⁴¹ ACF for $f(x) = |x|$ and leverage score are calculated but not used as a KPI.

Table 14: Model comparison for dataset SIM_GARCH2N30Y

Rank	Cat	Model	DIST	ACF	BT	Composite
1	HS	PHS	0.129	0.194	0.375	0.699
2	HS	FHS	0.487	0.761	0.303	1.551
3	NN	CGAN-FC	0.609	0.817	0.542	1.968
4	NN	CWGAN	0.804	0.650	0.516	1.970
5	PM	GARCHt-RET	0.947	0.670	0.496	2.113
6	NN	VAE	0.746	0.909	0.464	2.120
7	PM	GARCH-RET	0.904	0.689	0.535	2.128
8	PM	AR-RET	0.998	0.637	0.554	2.188
9	NN	DIFFUSION	0.975	0.865	0.615	2.455
10	NN	SIG	0.920	1.000	0.564	2.484
11	PM	AR	0.999	1.000	0.600	2.599
12	NN	CGAN-LSTM	0.991	0.900	0.806	2.697
13	PM	GARCH	1.000	1.000	0.913	2.913

KPI/score: the smaller the value, the better the model. KPIs are calculated for one dataset. DIST: distribution score, ACF: autocorrelation score, BT: backtesting score.

The models are tested using five simulated paths (five datasets) from AR(1)+GARCH with normal distribution for returns. Results for one path⁴² are presented in Table 14. This is a large table covering 13 models. Anticipating results later in the paper, we find that several models always perform badly for most datasets. Therefore, to save space, we present results for only a representative subset of seven models. These seven models include: (1) Plain historical simulation (PHS), which is simpler and performs better than FHS, (2) GARCH with conditional t distribution (GARCHt-RET), which performs better than GARCH with conditional normal distribution, (3) AR-RET, which is an autoregressive model without conditional heteroscedasticity, and (4) four NN models: CGAN-FC, CWGAN, SIG and VAE. The results for the complete list of models are available in an extended appendix (available on request). The shorter version of Table 14 is presented in Table 15

KPIs used in the table are described in Section 4.3. KPIs measure the distance (difference) between the synthetic data and real data. The smaller the KPI value, the better. Columns in the tables are:

1. Rank: model rank by composite score (the smaller, the better).
2. Cat: model category with historical simulation (HS), parametric model (PM) and neural network (NN)
3. Model: short model name

⁴²In the table caption, SIM_GARCH2N30Y means Path 2 with 30 year data simulated from GARCH-normal model.

Table 15: Model comparison for dataset SIM_GARCH2N30Y

Rank	Cat	Model	DIST	ACF	BT	Composite
1	HS	PHS	0.129	0.194	0.375	0.699
2	NN	CGAN-FC	0.609	0.817	0.542	1.968
3	NN	CWGAN	0.804	0.650	0.516	1.970
4	PM	GARCHt-RET	0.947	0.670	0.496	2.113
5	NN	VAE	0.746	0.909	0.464	2.120
6	PM	AR-RET	0.998	0.637	0.554	2.188
7	NN	SIG	0.920	1.000	0.564	2.484

KPI/score: the smaller the value, the better the model. KPIs are calculated for one dataset. DIST: distribution score, ACF: autocorrelation score, BT: backtesting score.

Table 16: Model ranking for dataset GARCH-normal

Rank	Cat	Model	DS1	DS2	DS3	DS4	DS5	AVG
1	HS	PHS	1	1	1	1	1	1.0
2	PM	GARCHt-RET	4	2	2	3	3	2.8
3	NN	CGAN-FC	2	6	6	2	4	4.0
4	PM	AR-RET	6	4	3	5	2	4.0
5	NN	CWGAN	3	5	5	4	5	4.4
6	NN	VAE	5	3	4	6	6	4.8
7	NN	SIG	7	7	7	7	7	7.0

4. DIST: distribution score

5. ACF: autocorrelation score

6. BT: backtest score.

7. Composite: composite score (DIST+ACF+BT)

The summary comparison across all five paths in Table 16. Tables for other paths are available in the extended appendix. Model ranking is based on Composite score. Table 16 shows the ranking of models for each of the five simulated datasets (paths) and the (arithmetic) average (AVG) ranking.

The results across the five simulated datasets have some variation and also consistency: Historical simulation (HS) methods are always ranked as the top model. HS is a commonly used VaR model among commercial banks. GARCHt-RET is ranked as the 2nd best model overall, but there is some variation in rank across datasets (e.g. #4 for dataset 1, and #2 for datasets 2 and 3).

Since the data are simulated using GARCH model, GARCH on returns (or GARCHt-RET) is the correctly specified model⁴³, which may which may explain its good performance. Even

⁴³Strictly speaking GARCH-normal (GARCH-RET) is the correctly specified model. GARCH-t distribution (GARCHt-RET) is a general case of GARCH-normal and can be loosely regarded as correctly specified.

Table 17: Model average sub-scores for dataset GARCH-normal

No.	Cat	Model	DIST	ACF	BT	Composite
1	HS	PHS	0.360	0.341	0.416	1.116
2	PM	GARCHt-RET	0.765	0.784	0.489	2.038
3	NN	CGAN-FC	0.714	0.878	0.579	2.171
4	NN	CWGAN	0.843	0.793	0.539	2.176
5	PM	AR-RET	0.999	0.622	0.564	2.185
6	NN	VAE	0.792	0.940	0.498	2.230
7	NN	SIG	0.894	1.000	0.563	2.457

KPI/score: the smaller the value, the better the model. These scores/subscores are the average scores across five datasets. DIST: distribution score, ACF: autocorrelation score, BT: backtesting score.

though GARCHt-RET is the correctly specified model, it does not beat PHS performance because of the noise from the (GARCH) parameter estimation.

AR on returns (AR-NET) shares the AR part with the GARCH model, but it does not have conditional heteroscedasticity. It is ranked the 4th model in performance.

CGAN-FC is ranked the 3rd model in performance, better than the AR-RET model, and the other three NN models.

In the table above, the ranking is based on Composite score for each individual dataset. In Table 17, we present the average subscore in each performance (or KPI) category as well as the composite score across five datasets. The model ranking based on subscores is presented in Table 18, which has model **ranking by average subscores** across datasets rather than **average ranking** across datasets as in Table 16 . By looking at ranking based on subscores, we can find whether a model’s overall rank is consistent across subscores, or whether good performance in one category is offset by bad performance in another category. Since different models capture the relationships in the data differently, we expect some variation of ranking by subscores ⁴⁴ , otherwise columns in Table 16 would always show the same rankings.

Table 17 shows that (1) DIST and ACF scores have similar ranges (DIST: 0.360-0.999, ACF: 0.341-1.0), while BT has a smaller range (0.416-0.579). This indicates that the models do not have much differentiation in backtest (BT) performance; (2) PHS performs especially well in Distribution and ACF, which guarantees its final ranking of being the best model (Table 18). (3) CGAN-FC is ranked quite well by Distribution (#2) but ranked #7 by backtesting (BT). (4) The performance of CWGAN model follows right after the CGAN-FC model. (5) AR-RET is ranked very badly by Distribution (#7), and is ranked very well by ACF (#2). AR-RET tracks ACF well by the nature of AR model.

⁴⁴e.g. some models may capture correlation better, while others may capture distribution better.

Table 18: Model ranking by average sub-score for dataset GARCH-normal

Cat	Model	Rank_DIST	Rank_ACF	Rank_BT	Rank
HS	PHS	1	1	1	1
PM	GARCHt-RET	3	3	2	2
NN	CGAN-FC	2	5	7	3
NN	CWGAN	5	4	4	4
PM	AR-RET	7	2	6	5
NN	VAE	4	6	3	6
NN	SIG	6	7	5	7

Model rank by subscores. The lower the rank, the better the model. Rank_DIST: rank by distribution (DIST), Rank_ACF: rank by ACF score, Rank_BT: rank by backtesting score (BT), Rank: rank by composite score.

Table 19: Model comparison for dataset SIM_GARCH2T5CR30Y

Rank	Cat	Model	DIST	ACF	BT	Composite
1	HS	PHS	0.364	0.200	0.429	0.993
2	PM	GARCHt-RET	0.830	0.795	0.445	2.071
3	NN	CWGAN	0.819	0.819	0.502	2.141
4	NN	CGAN-FC	0.853	0.776	0.593	2.222
5	PM	AR-RET	1.000	0.717	0.568	2.285
6	NN	VAE	0.886	0.997	0.500	2.384
7	NN	SIG	0.994	1.000	0.572	2.567

KPI/score: the smaller the value, the better the model. KPIs are calculated for one dataset. DIST: distribution score, ACF: autocorrelation score, BT: backtesting score.

4.4.2 Results using simulated GARCH-t(5) Dataset

The models are run for five paths simulated from AR(1)+GARCH and t distribution with 5 degrees of freedom. Compared with GARCH with normal distribution, GARCH with t(5) distribution has fat tails. Similar to the analysis for GARCH-normal datasets, results for one path are presented in Tables 19, with summary results across all five paths in Table 20, average subscores and corresponding model ranking in Tables 21 and 22.

The results are similar to those for GARCH-normal simulated data in the last subsection.

4.4.3 Results using simulated GARCH-t(3) Dataset

The models are run for five paths simulated from AR(1)+GARCH and t distribution with 3 degrees of freedom. Compared with GARCH-normal and GARCH-t(5), GARCH with t(3) distribution has much fatter tails. Similar to the analysis for GARCH-normal datasets, results for one path are presented in Tables 23, with summary results across all five paths in Table 24, average subscores and model ranking in Tables 25 and 26.

The results are similar to those for GARCH-normal and GARCH-t(5) simulated data in the

Table 20: Model ranking for dataset GARCH-t(5)

Rank	Cat	Model	DS1	DS2	DS3	DS4	DS5	AVG
1	HS	PHS	1	1	1	1	1	1.0
2	PM	GARCHt-RET	2	2	2	2	2	2.0
3	NN	CGAN-FC	4	4	4	3	3	3.6
4	NN	CWGAN	3	5	3	4	4	3.8
5	PM	AR-RET	5	3	6	7	5	5.2
6	NN	VAE	6	6	5	5	6	5.6
7	NN	SIG	7	7	7	6	7	6.8

Table 21: Model average sub-scores for dataset GARCH-t(5)

No.	Cat	Model	DIST	ACF	BT	Composite
1	HS	PHS	0.373	0.336	0.421	1.130
2	PM	GARCHt-RET	0.743	0.797	0.415	1.955
3	NN	CGAN-FC	0.784	0.786	0.590	2.160
4	NN	CWGAN	0.909	0.796	0.508	2.213
5	PM	AR-RET	1.000	0.745	0.565	2.310
6	NN	VAE	0.907	0.992	0.510	2.410
7	NN	SIG	0.983	0.978	0.566	2.526

KPI/score: the smaller the value, the better the model. These scores/subscores are the average scores across five datasets. DIST: distribution score, ACF: autocorrelation score, BT: backtesting score.

Table 22: Model ranking by average sub-score for dataset GARCH-t(5)

Cat	Model	Rank_DIST	Rank_ACF	Rank_BT	Rank
HS	PHS	1	1	2	1
PM	GARCHt-RET	2	5	1	2
NN	CGAN-FC	3	3	7	3
NN	CWGAN	5	4	3	4
PM	AR-RET	7	2	5	5
NN	VAE	4	7	4	6
NN	SIG	6	6	6	7

Model rank by subscores. The lower the rank, the better the model. Rank_DIST: rank by distribution (DIST), Rank_ACF: rank by ACF score, Rank_BT: rank by backtesting score (BT), Rank: rank by composite score.

Table 23: Model comparison for dataset SIM_GARCH2T3CR30Y

Rank	Cat	Model	DIST	ACF	BT	Composite
1	HS	PHS	0.340	0.414	0.311	1.064
2	PM	GARCHt-RET	0.845	0.741	0.455	2.042
3	NN	CWGAN	0.975	0.808	0.556	2.340
4	NN	CGAN-FC	0.946	0.900	0.568	2.414
5	PM	AR-RET	1.000	0.849	0.569	2.418
6	NN	VAE	0.999	0.999	0.482	2.479
7	NN	SIG	0.990	1.000	0.569	2.559

KPI/score: the smaller the value, the better the model. KPIs are calculated for one dataset. DIST: distribution score, ACF: autocorrelation score, BT: backtesting score.

Table 24: Model ranking for dataset GARCH-t(3)

Rank	Cat	Model	DS1	DS2	DS3	DS4	DS5	AVG
1	HS	PHS	1	1	1	1	1	1.0
2	PM	GARCHt-RET	2	2	2	2	2	2.0
3	NN	CGAN-FC	4	3	3	4	3	3.4
4	NN	CWGAN	3	5	6	3	6	4.6
5	PM	AR-RET	5	4	5	5	4	4.6
6	NN	VAE	6	6	4	6	5	5.4
7	NN	SIG	7	7	7	7	7	7.0

last subsections.

We conjecture that the much fat tail in the $t(3)$ distribution may have caused disruption to model training and performance.

4.4.4 Results using simulated CIR dataset

The models are run for five simulated paths from CIR model. Similar set of tables are presented: the results for one path in Tables 27, summary of rankings across all five paths in Table 28, the average subscores in Tables 29 and model ranking based on average subscores in Table 30.

There are some similarities and differences from the results for GARCH datasets. (1) HS model is the top performers consistently across the five paths (Table 28) and across subscore categories (Table 30). (2) GARCHt-NET is the 2nd best model. (3) AR-NET is ranked #3rd (both Tables 28 and 30) and performs better than NN models (only slightly better than CWGAN with scores 2.115 and 2.181 in Tables 25).

Table 25: Model average sub-scores for dataset GARCH-t(3)

No.	Cat	Model	DIST	ACF	BT	Composite
1	HS	PHS	0.432	0.394	0.360	1.186
2	PM	GARCHt-RET	0.754	0.781	0.456	1.990
3	NN	CGAN-FC	0.774	0.806	0.564	2.144
4	NN	CWGAN	0.870	0.866	0.545	2.282
5	PM	AR-RET	1.000	0.743	0.568	2.311
6	NN	VAE	0.873	0.943	0.496	2.312
7	NN	SIG	0.966	0.976	0.583	2.524

KPI/score: the smaller the value, the better the model. These scores/subscores are the average scores across five datasets. DIST: distribution score, ACF: autocorrelation score, BT: backtesting score.

Table 26: Model ranking by average sub-score for dataset GARCH-t(3)

Cat	Model	Rank_DIST	Rank_ACF	Rank_BT	Rank
HS	PHS	1	1	1	1
PM	GARCHt-RET	2	3	2	2
NN	CGAN-FC	3	4	5	3
NN	CWGAN	4	5	4	4
PM	AR-RET	7	2	6	5
NN	VAE	5	6	3	6
NN	SIG	6	7	7	7

Model rank by subscores. The lower the rank, the better the model. Rank_DIST: rank by distribution (DIST), Rank_ACF: rank by ACF score, Rank_BT: rank by backtesting score (BT), Rank: rank by composite score.

Table 27: Model comparison for dataset SIM_CIRS1bi

Rank	Cat	Model	DIST	ACF	BT	Composite
1	HS	PHS	0.071	0.411	0.456	0.938
2	NN	CWGAN	0.724	0.653	0.556	1.934
3	PM	GARCHt-RET	0.709	0.761	0.469	1.939
4	PM	AR-RET	0.891	0.528	0.564	1.983
5	NN	CGAN-FC	0.996	0.407	0.606	2.009
6	NN	SIG	0.928	0.747	0.566	2.241
7	NN	VAE	0.881	0.791	0.595	2.268

KPI/score: the smaller the value, the better the model. KPIs are calculated for one dataset. DIST: distribution score, ACF: autocorrelation score, BT: backtesting score.

Table 28: Model ranking for dataset CIR

Rank	Cat	Model	DS1	DS2	DS3	DS4	DS5	AVG
1	HS	PHS	1	1	1	1	2	1.2
2	PM	GARCHt-RET	3	2	2	2	1	2.0
3	PM	AR-RET	4	3	3	5	3	3.6
4	NN	CWGAN	2	4	4	6	6	4.4
5	NN	CGAN-FC	5	6	7	3	5	5.2
6	NN	VAE	7	7	5	4	4	5.4
7	NN	SIG	6	5	6	7	7	6.2

Table 29: Model average sub-scores for dataset CIR

No.	Cat	Model	DIST	ACF	BT	Composite
1	HS	PHS	0.382	0.378	0.489	1.249
2	PM	GARCHt-RET	0.639	0.615	0.481	1.735
3	PM	AR-RET	0.969	0.571	0.575	2.115
4	NN	CWGAN	0.900	0.709	0.572	2.181
5	NN	VAE	0.908	0.758	0.579	2.245
6	NN	CGAN-FC	0.946	0.701	0.616	2.263
7	NN	SIG	0.981	0.796	0.585	2.362

KPI/score: the smaller the value, the better the model. These scores/subscores are the average scores across five datasets. DIST: distribution score, ACF: autocorrelation score, BT: backtesting score.

Table 30: Model ranking by average sub-score for dataset CIR

Cat	Model	Rank_DIST	Rank_ACF	Rank_BT	Rank
HS	PHS	1	1	2	1
PM	GARCHt-RET	2	3	1	2
PM	AR-RET	6	2	4	3
NN	CWGAN	3	5	3	4
NN	VAE	4	6	5	5
NN	CGAN-FC	5	4	7	6
NN	SIG	7	7	6	7

Model rank by subscores. The lower the rank, the better the model. Rank_DIST: rank by distribution (DIST), Rank_ACF: rank by ACF score, Rank_BT: rank by backtesting score (BT), Rank: rank by composite score.

4.4.5 Summary

Results for simulated GARCH (with Normal and t distribution with 3 and 5 degrees of freedom) and CIR datasets can be summarized as follows.

Plain historical simulation (PHS) model is the top performer for all 4 DGPs.

GARCH with t distribution (GARCHt-NET) model is the 2nd best model.

CWGAN and CGAN-FC are the better performing NN models.

4.5 Results using historical data

There are three sets of USD yield curve data, USDYC1 (Libor curve 2008-2022), USDYC2 (Par yield 2008-2023) and USDYC3 (Par yield 2000-2023). See details in Sections 3.1. This section shows a summary of the results. More detailed results are available in an extended appendix (available upon request).

KPIs measure the distance (difference) between the synthetic data and real data. The smaller the KPI value, the better. See Section refsubsec:evaluation metrics for details.

4.5.1 Results of model runs

There are three sets of tables for results. (1) Results for each dataset, Tables 31 for USDYC1, Tables 32 for USDYC2 and Table 33 for USDYC3. (2) A summary of rankings across the three datasets is presented in Table 34. (3) The average subscores across the three datasets are presented in Table 35 and ranking by subscores in Table 36.

Observations are based mainly on Tables 34 and 36.

HS model performs the best, followed by GARCHt-RET model.

CWGAN is the top performing NN model, followed by VAE and SIG models.

The simple AR-RET model has very decent performance and is ranked only after the best NN model (CWGAN).

The difference between AR-RET and GARCHt-RET models is the GARCH dynamics of conditional variance for the errors of AR(1) model. The results show that modeling the GARCH effect (in returns) is important.

Recall that for simulated data, the simple CGAN-FC has comparable performance to CWGAN. But for the USD yield curve, CGAN-FC has the worst performance.

Additional model runs are made for USDYC1 dataset with 1-year condition in NN models. The results in Appendix A.2 show that, with much more parameters, the NN models do not improve in performance.

Table 31: Model comparison for dataset USDYC1 (Libor curve)

Rank	Cat	Model	DIST	ACF	BT	Composite
1	HS	PHS	0.197	0.750	0.537	1.484
2	PM	GARCHt-RET	0.734	0.789	0.545	2.068
3	NN	CWGAN	0.766	0.764	0.565	2.094
4	NN	SIG	0.807	0.876	0.551	2.234
5	PM	AR-RET	0.971	0.706	0.572	2.248
6	NN	VAE	0.997	0.931	0.556	2.484
7	NN	CGAN-FC	0.991	0.814	0.806	2.611

KPI/score: the smaller the value, the better the model. KPIs are calculated for one dataset.
DIST: distribution score, ACF: autocorrelation score, BT: backtesting score.

Table 32: Model comparison for dataset USDYC2 (Par curve 2008-2023)

Rank	Cat	Model	DIST	ACF	BT	Composite
1	HS	PHS	0.328	0.792	0.552	1.673
2	PM	GARCHt-RET	0.837	0.824	0.538	2.199
3	NN	CWGAN	0.920	0.776	0.552	2.249
4	PM	AR-RET	0.958	0.829	0.581	2.368
5	NN	VAE	0.990	0.812	0.567	2.369
6	NN	SIG	0.956	0.876	0.573	2.406
7	NN	CGAN-FC	0.998	0.857	0.917	2.772

KPI/score: the smaller the value, the better the model. KPIs are calculated for one dataset.
DIST: distribution score, ACF: autocorrelation score, BT: backtesting score.

Table 33: Model comparison for dataset USDYC3 (Par curve 2000-2023)

Rank	Cat	Model	DIST	ACF	BT	Composite
1	HS	PHS	0.128	0.594	0.540	1.261
2	PM	GARCHt-RET	0.831	0.844	0.542	2.217
3	NN	CWGAN	0.959	0.815	0.553	2.327
4	NN	VAE	0.998	0.817	0.586	2.401
5	PM	AR-RET	0.974	0.844	0.586	2.405
6	NN	SIG	0.962	0.945	0.562	2.469
7	NN	CGAN-FC	0.965	0.951	0.710	2.626

KPI/score: the smaller the value, the better the model. KPIs are calculated for one dataset.
DIST: distribution score, ACF: autocorrelation score, BT: backtesting score.

Table 34: Model ranking for dataset USDYC

Rank	Cat	Model	USDYC1	USDYC2	USDYC3	AVG
1	HS	PHS	1	1	1	1.0
2	PM	GARCHt-RET	2	2	2	2.0
3	NN	CWGAN	3	3	3	3.0
4	PM	AR-RET	5	4	5	4.7
5	NN	VAE	6	5	4	5.0
6	NN	SIG	4	6	6	5.3
7	NN	CGAN-FC	7	7	7	7.0

Table 35: Model average sub-scores for dataset USDYC

No.	Cat	Model	DIST	ACF	BT	Composite
1	HS	PHS	0.218	0.712	0.543	1.473
2	PM	GARCHt-RET	0.801	0.819	0.542	2.161
3	NN	CWGAN	0.882	0.785	0.557	2.223
4	PM	AR-RET	0.968	0.793	0.580	2.340
5	NN	SIG	0.908	0.899	0.562	2.370
6	NN	VAE	0.995	0.853	0.570	2.418
7	NN	CGAN-FC	0.984	0.874	0.811	2.669

KPI/score: the smaller the value, the better the model. These scores/subscores are the average scores across five datasets. DIST: distribution score, ACF: autocorrelation score, BT: backtesting score.

Table 36: Model ranking by average sub-score for dataset USDYC

Cat	Model	Rank_DIST	Rank_ACF	Rank_BT	Rank
HS	PHS	1	1	2	1
PM	GARCHt-RET	2	4	1	2
NN	CWGAN	3	2	3	3
PM	AR-RET	5	3	6	4
NN	SIG	4	7	4	5
NN	VAE	7	5	5	6
NN	CGAN-FC	6	6	7	7

Model rank by subscores. The lower the rank, the better the model. Rank_DIST: rank by distribution (DIST), Rank_ACF: rank by ACF score, Rank_BT: rank by backtesting score (BT), Rank: rank by composite score.

Table 37: Model ranking for dataset USD_YC with different random seeds

Cat	Model	rand1	rand2	rand3	rand4	rand5	AVG
HS	PHS	1	1	1	1	1	1.0
PM	GARCHt-RET	2	4	2	2	2	2.4
NN	CWGAN	3	2	4	3	3	3.0
PM	AR-RET	5	3	5	4	4	4.2
NN	SIG	4	6	3	5	6	4.8
NN	VAE	6	5	6	6	5	5.6
NN	CGAN-FC	7	7	7	7	7	7.0

Table 38: Model average sub-scores for dataset USDYC (rand)

No.	Cat	Model	DIST	ACF	BT	Composite
1	HS	PHS	0.304	0.733	0.537	1.574
2	PM	GARCHt-RET	0.749	0.792	0.544	2.085
3	NN	CWGAN	0.859	0.780	0.551	2.189
4	PM	AR-RET	0.968	0.718	0.570	2.256
5	NN	SIG	0.916	0.858	0.561	2.335
6	NN	VAE	0.987	0.898	0.564	2.449
7	NN	CGAN-FC	0.949	0.785	0.830	2.564

KPI/score: the smaller the value, the better the model. These scores/subscores are the average scores across five model runs with different random seeds. DIST: distribution score, ACF: autocorrelation score, BT: backtesting score.

4.5.2 Additional results with random seeds

Randomization is used in several steps in model training and testing. For example, random selection is used in train-test split; it may also be used in model training for batch normalization and forming batches for some NN models; random numbers are used in generation and backtesting steps.

To assess the impact of random seeds on the models, additional model runs are made with different random seeds for USDYC1. Summary of results across five random seeds are presented in Table 37. Earlier results in Tables 31 is just one set of results with a specific set of random seed.

There is some variation across the runs. HS is the best model for all five random seeds. GARCHt-RET is the 2nd best model for all but the 2nd seed. The ranking of models for the top four models are consistent with the three USD yield curves in Table 34 and 36.

Average subscores across random seeds are presented Tables 38 with ranking results in Table 39 The results are consistent with Table 37.

Table 39: Model ranking by average sub-score for dataset USDYC (rand)

Cat	Model	Rank_DIST	Rank_ACF	Rank_BT	Rank
HS	PHS	1	2	1	1
PM	GARCHt-RET	2	5	2	2
NN	CWGAN	3	3	3	3
PM	AR-RET	6	1	6	4
NN	SIG	4	6	4	5
NN	VAE	7	7	5	6
NN	CGAN-FC	5	4	7	7

Model rank by subscores. The lower the rank, the better the model. Rank_DIST: rank by distribution (DIST), Rank_ACF: rank by ACF score, Rank_BT: rank by backtesting score (BT), Rank: rank by composite score.

Table 40: Model comparison for dataset MRDATA

Rank	Cat	Model	DIST	ACF	BT	Composite
1	HS	PHS	0.365	0.804	0.384	1.552
2	PM	GARCHt-RET	0.813	0.829	0.502	2.144
3	NN	CWGAN	0.793	0.835	0.535	2.163
4	NN	VAE	0.883	0.849	0.612	2.345
5	NN	SIG	0.923	0.921	0.568	2.412
6	NN	CGAN-FC	0.934	0.837	0.644	2.415
7	PM	AR-RET	0.992	0.866	0.572	2.430

KPI/score: the smaller the value, the better the model. KPIs are calculated for one dataset. DIST: distribution score, ACF: autocorrelation score, BT: backtesting score.

4.5.3 Results with a market risk dataset

For further testing, we compile another dataset for market risk, which includes eight key time series spanning the period 2007-2022: SPX and VIX for equity market, 3M and 10Y forward Treasury rates for fixed income market, North American CDX IG and HY for credit market, USD/EUR exchange rate for foreign exchange market, 1M Oil futures for commodity. For this dataset, log returns are calculated for four variables SPX, VIX, USD/EUR and Oil, and absolute returns are calculated for the rest four variable ⁴⁵. The results are presented in Table 40. The results are broadly consistent with those for the USDYC datasets in the sense that the top three models are the same. The difference from the results of USDYC dataset is that the AR-RET model performs well for USDYC dataset but it does not perform well for this market risk dataset.

⁴⁵Logs of the level for the four variables SPX, VIX, USD/EUR and Oil are saved into the input dataset and the models are run as if absolute return is appropriate for all eight variables in the dataset.

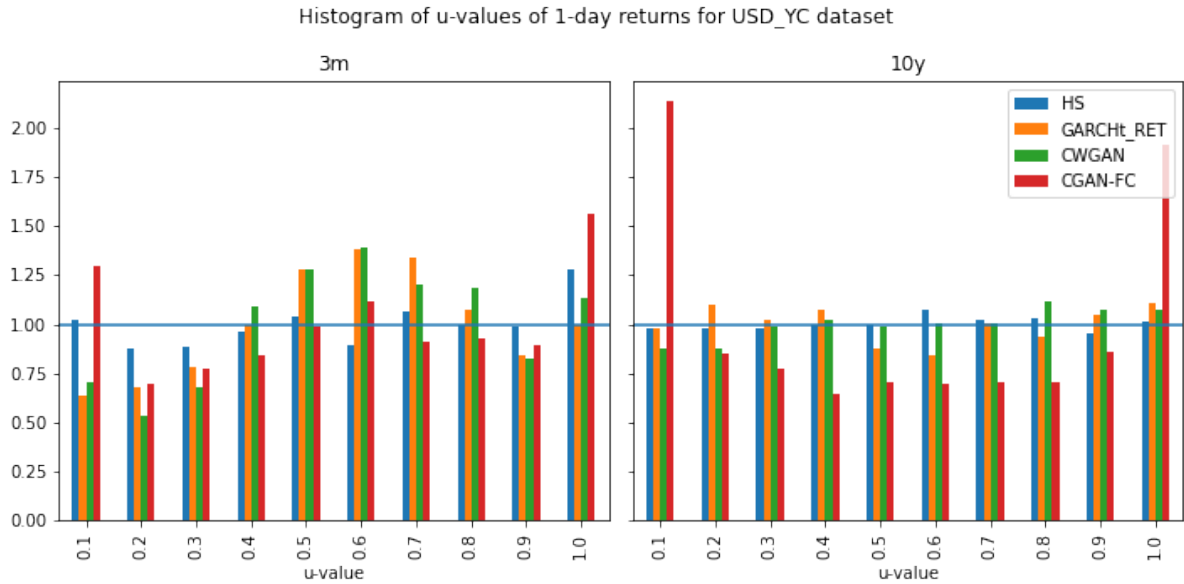


Figure 16: Histogram of u-values

4.5.4 Rationalization of results

4.5.4.1 Histogram of u-values The model ranking for both simulated and historical datasets are based on KPIs (or scores) that capture different aspects of model comparison. The KPIs are calculated through multiple steps of combination (or aggregation) of individual scores.

To rationalize the results, we do additional analysis for four selected models, PHS, GARCH_RET, CWGAN and NelsonSiegel model (NS) and shed more light on the model ranking and on the model features behind the KPIs. We recall several key quantities for backtesting.

For each business date t in the backtest period, a condition (e.g. the previous 10 day's returns in period $t - 10$ to $t - 1$) is used along with a set of random numbers to generate a return distribution for every day in the next 10 days (including t). The realized value x_t is compared with the generated distribution for time t , \tilde{x}_t , to calculate a u-value, $u_t = \hat{F}_t(x_t)$, where \hat{F}_t is the generated distribution. u-values, as probabilities, range from 0 to 1. Histogram of u-values are presented in Figure 16. For a true model (or true distribution \hat{F}_t), the u-values should follow a uniform distribution, and the histogram should be flat at 1.0. The following observations can be made based on Figure 16:

- As the tenor gets longer, the histogram gets closer to uniform and there are less difference among the models (except for CGAN-FC).
- Even for the top three models, the histogram seems rugged and different from uniform. Statistical test for the null hypothesis of uniform distribution belong to formal model backtesting and is beyond the scope of this paper.

4.5.4.2 Envelope coverage The realized value x_t , and the 5% and 95% quantiles of the forecast distribution are plotted for every business date in the backtest period. This is called an envelope plot, and it shows how well the generated distribution covers the realized returns. Figure 17 shows the envelope plot for 3M tenor and Figure 18 for 10Y tenor. The following observations can be made:

- The upper (95%) and lower (5%) quantiles for NN models (CWGAN) have very noisy day to day changes.
- The upper (95%) and lower (5%) quantiles for HS and GARCHt-RET models and are less noisy and show clear trends over time corresponding to market episodes.
- For 3M tenor, the upper quantiles for NN models become negative during the COVID-19 pandemic. It is likely that, since the NN models depend on the condition (lagged values), when the condition has large values, the NN model prediction breaks down because there are not many such episodes in the training data.
- The envelope plots for 10Y tenor is better and there is cleaner separation of upper and lower quantiles, since 10Y data are more stable and less challenging to model.
- In the plot, we also show the breach rates for 5% and 95% quantiles. For example, for GARCHt-RET model for 3m tenor, the meaning of “at 5%=2.2, 4.6, 3.4” is, (1) in the first half of the date range (2008-2016, or first sub-period), 2.2% of the realized return is lower than the 5% quantile. (2) In the second half of the date range (2016-2022, or second sub-period), the breach rate is 4.6%. (3) In the whole date range, the breach rate is 3.4%. For the true model, the breach rate should be 5%. Thus the difference between the realized and expected breach rate (5%) shows deviation of the model from the true model. The breach rates for 95% quantile are displayed similarly and show that the breach rates are close to 5%.
- For CWGAN model, the breach rates in the first sub-period (1.6%) is much lower than 5%, and those in the second sub-period (7.7%) are much higher than 5%, with the overall breach rates being much close to 5%. This serves as a reminder than sub-period analysis is important for studying model behavior.

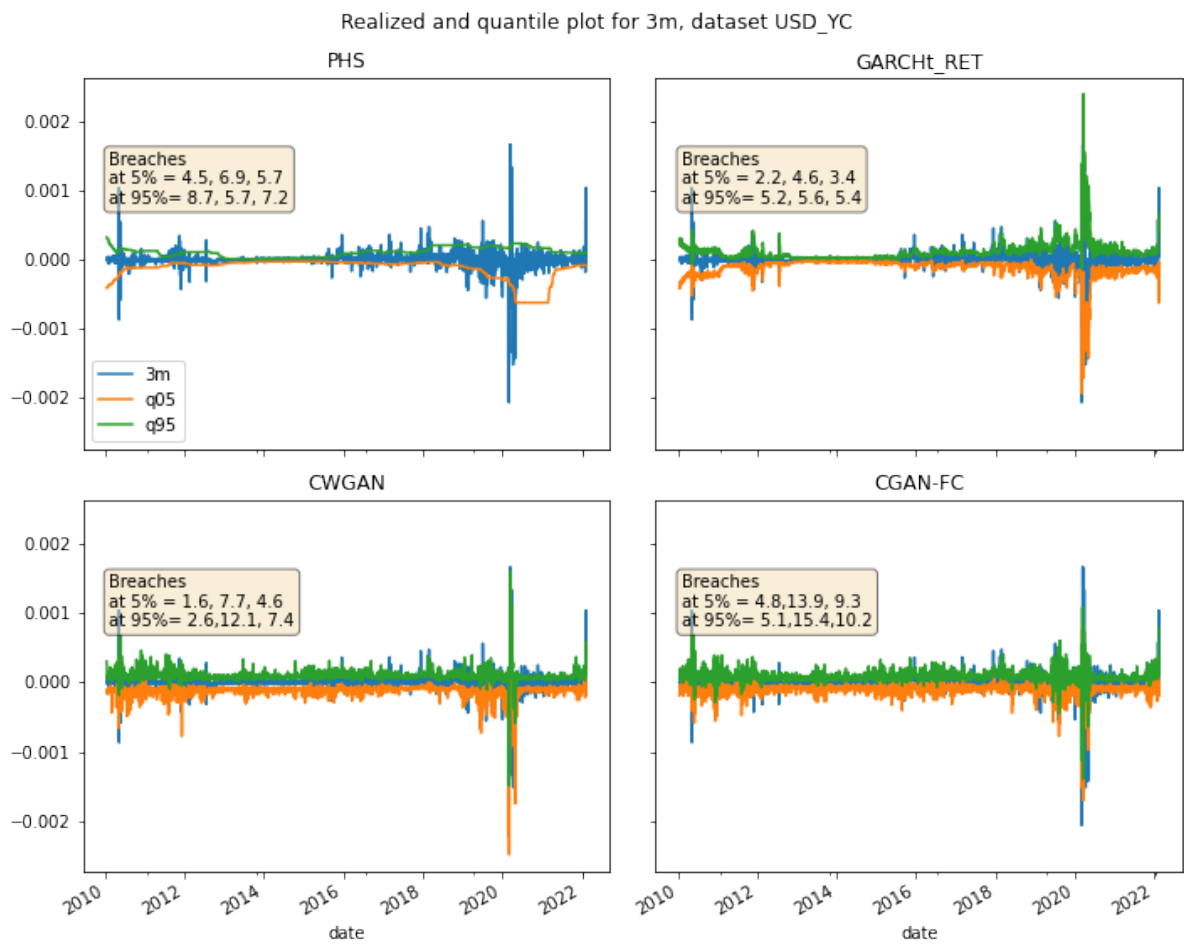


Figure 17: Envelope plot of 3M, USD_YC

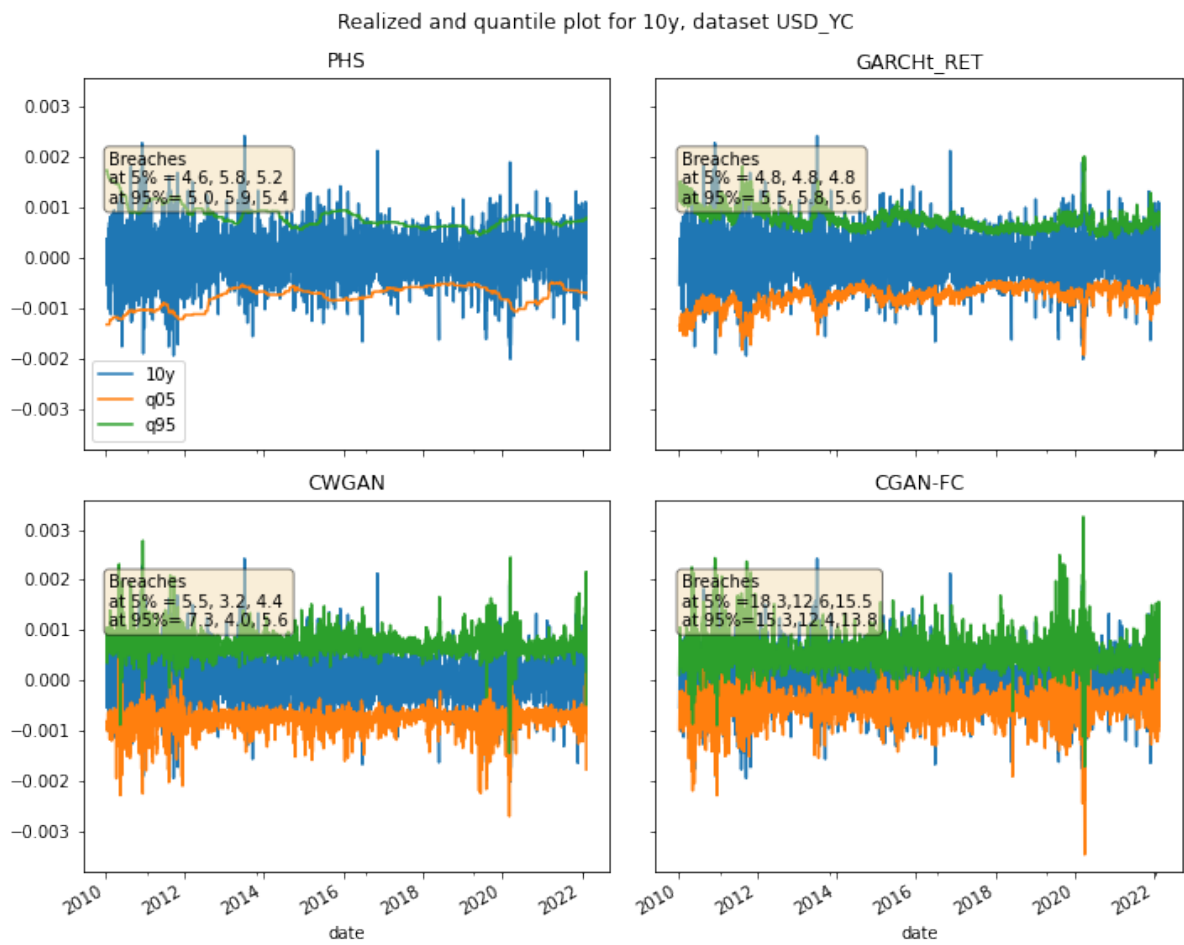


Figure 18: Envelope plot of 10Y, USD_YC

5 Conclusion and future work

This paper provides a comparative review of models for short horizon distribution forecasting, covering historical simulation models, parametric models as well as deep generative (NN) models. Model testing is conducted on both simulated and real-world historical data. The hyperparameters are set so that the performance ranking can be done consistently across all models. Comprehensive measures of model performance and aggregation of KPI schema are designed carefully to capture key features financial time series.

The findings can be summarized as follows. (1) HS model perform the best across all simulated and historical datasets used in model testing. HS VaR models are currently in use by many commercial banks, thus are included for comparison with parametric and NN models. The limitation of HS models is that all future scenarios are drawn from and thus limited to realized historical scenarios. The simple implementation of HS models do not generate a desired variety of future scenarios. (2) GARCH model (for returns, with conditional t distribution in particular) is consistently the best parametric model, and ranked only behind HS model. GARCH model captures volatility clustering, which is a salient feature of financial time series. AR-RET also has good performance for some datasets, but not as good as GARCH-RET model. (3) CWGAN is consistently the best performing deep generative model across different datasets. (4) Other deep learning models such as SIG, CGAN and VAE also have good performance for some datasets, however the performance is not consistent across all datasets. (5) Simulated data from GARCH and t distribution with three degrees of freedom have very different model ranking from other datasets. This may be due to the very fat tails of the simulated data.

The contributions of our study include:

- A comprehensive review of three categories of models (historical simulation, parametric and deep generative models).
- Innovations of deep learning methodologies, namely Encoder-Decoder CGAN (CGAN-LSTM) and continuous-conditional VAE.
- A complete review of a collection of KPIs, and designed schema to combine KPIs.
- Consistent model testing and performance ranking using simulated and real-world data.

Future work includes the following areas: (1) Expand the model list to include other NN architectures such as transformers; (2) Implement NN models such as Tail-GAN (Cont et al. (2023)) that can improve modeling of the tails of the distribution; (3) Research on distribution forecasting for longer risk horizons, such as 5-, 10- and even 30-years; (4) Improve ways to integrate KPI's, such as KPIs for data variability and variety.

Authors' affiliation and contacts: all authors are with Wells Fargo. Authors' email contacts

are:

Lars Ericson: Lars.Ericson@wellsfargo.com

Xuejun Zhu: Xuejun.Zhu@wellsfargo.com

Xusi Han: Xusi.Han@wellsfargo.com

Rao Fu: Rao.Fu@wellsfargo.com

Shuang Li: Shuang.Li2@wellsfargo.com

Steve Guo*: Steve.Guo@wellsfargo.com, corresponding author

Ping Hu: Ping.Hu@wellsfargo.com

References

- Arjovsky, M., S. Chintala, and L. Bottou (2017). Wasserstein gan. <https://arxiv.org/abs/1701.07875>.
- BARONE-ADESI, G. and K. GIANNOPOULOS (2001). Non-parametric var techniques. myths and realities. *Economic Notes by Banca Monte dei Paschi di Siena SpA* 30(2), 167–181.
- Barone-Adesi, G., K. Giannopoulos, and L. Vosper (1999). Var without correlations for portfolios of derivatives securities. *Journal of Futures Markets* 19, 583–602.
- Basel Committee on Banking Supervision (2019). Minimum capital requirements for market risk. *Bank for international settlements*.
- Berkowitz, J. (2001). Testing density forecasts, with applications to risk management. *Journal of Business & Economic Statistics* 19(4), 465–474.
- Bollerslev, T. (1986). Generalized Autoregressive Conditional Heteroskedasticity. *Journal of Economics* 31(3), 307–327.
- Brophy, E., Z. Wang, Q. She, and T. Ward (2021). Generative adversarial networks in time series: A survey and taxonomy. <https://arxiv.org/abs/2107.11098>.
- Brophy, E., Z. Wang, Q. She, and T. Ward (2023, feb). Generative adversarial networks in time series: A systematic literature review. *ACM Comput. Surv.* 55(10). <https://doi.org/10.1145/3559540>.
- Chevyrev, I. and A. Kormilitzin (2016). A primer on the signature method in machine learning. *arXiv preprint arXiv:1603.03788*.
- Cont, R., M. Cucuringu, R. Xu, and C. Zhang (2023). Tail-gan: Learning to simulate tail risk scenarios.
- Cox, J. C., J. E. Ingersoll, and S. A. Rossi (1985). A Theory of the Term Structure of Interest Rates. *Econometrica* 53(2), 385–407.
- Crnkovic, C. and J. Drachman (1996). Quality control. *Risk* 9(9), 138–143.
- Desai, A., C. Freeman, Z. Wang, and I. Beaver (2021). Timevae: A variational auto-encoder for multivariate time series generation. <https://arxiv.org/abs/2111.08095>.

- Dhariwal, P. and A. Nichol (2021). Diffusion models beat gans on image synthesis. In M. Ranzato, A. Beygelzimer, Y. Dauphin, P. Liang, and J. W. Vaughan (Eds.), *Advances in Neural Information Processing Systems*, Volume 34, pp. 8780–8794. Curran Associates, Inc. <https://proceedings.neurips.cc/paper/2021/file/49ad23d1ec9fa4bd8d77d02681df5cfa-Paper.pdf>.
- Dickey, D. and W. Fuller (1979). Distribution of the estimators for autoregressive time series with a unit root. *Journal of the American Statistical Association* 74(366), 427–431.
- Diebold, F. X. and C. Li (2006). Forecasting the Term Structure of Government Bond Yields. *Journal of Economics* 130(2), 337–364.
- Dragulescu, A. A. and V. M. Yakovenko (2002). Probability distribution of returns in the heston model with stochastic volatility. <https://arxiv.org/abs/cond-mat/0203046>.
- Engle, R. F. (1982). "autoregressive conditional heteroskedasticity with estimates of the variance of United Kingdom inflation". *Econometrica* 50(4), 987–1007.
- Fu, R. (2022). An introduction of encoder-and-decoder cgan framework.
- Fu, R., J. Chen, S. Zeng, Y. Zhuang, and A. Sudjianto (2019). Time series simulation by conditional generative adversarial net. <https://arxiv.org/abs/1904.11419>.
- Graves, A. (2013). Generating sequences with recurrent neural networks. <https://arxiv.org/abs/1308.0850>.
- Ho, J., A. Jain, and P. Abbeel (2020). Denoising diffusion probabilistic models. In H. Larochelle, M. Ranzato, R. Hadsell, M. Balcan, and H. Lin (Eds.), *Advances in Neural Information Processing Systems*, Volume 33, pp. 6840–6851. Curran Associates, Inc. <https://proceedings.neurips.cc/paper/2020/file/4c5bcfec8584af0d967f1ab10179ca4b-Paper.pdf>.
- Johnson, S. (2020). Synthetic data for finance - from theory to practice. https://www.ubs.com/global/en/investment-bank/in-focus/research-focus/quant-answers/quant-insight-series/_jcr_content/mainpar/toplevelgrid_7262680_322968126_col3/actionbutton_3358030.0949818704.file/PS9jb250ZW50L2RhbS9pbmRlcm5ldGhvc3Rpbmcvaw52ZXN0bWVudGJhbmsvZW4vZXF=/synthetic-data-for-finance-stefan-jansen-ubs-2021.pdf.
- Kingma, D. P. and M. Welling (2019). An introduction to variational autoencoders. *Foundations and Trends® in Machine Learning* 12(4), 307–392. <https://doi.org/10.1561%2F22000000056>.
- Kuznetsov, V. and Z. Mariet (2018). Foundations of sequence-to-sequence modeling for time series. <https://arxiv.org/abs/1805.03714>.
- McInnes, L., J. Healy, and J. Melville (2020). Umap: Uniform manifold approximation and projection for dimension reduction.

- Morrill, J., A. Fermanian, P. Kidger, and T. Lyons (2020). A generalised signature method for multivariate time series feature extraction. *arXiv preprint arXiv:2006.00873*.
- Nelson, C. R. and A. F. Siegel (1987). Parsimonious modeling of yield curve. *Journal of Business* 60, 473–489.
- Perignon, C. and D. R. Smith (2010). The level and quality of value-at-risk disclosure by commercial banks. *Journal of Banking & Finance* 34(2), 362–377.
- Ramdas, A., N. Garcia, and M. Cuturi (2015). On wasserstein two sample testing and related families of nonparametric tests. <https://arxiv.org/abs/1509.02237>.
- Ramya Malur Srinivasan, A. C. (2020). Generating user-friendly explanations for loan denials using generative adversarial networks. <https://www.risk.net/investing/quant-investing/7833326/in-fake-data-quants-see-a-fix-for-backtesting>.
- Rasul, K., C. Seward, I. Schuster, and R. Vollgraf (2021). Autoregressive denoising diffusion models for multivariate probabilistic time series forecasting. <https://arxiv.org/abs/2101.12072>.
- Sabaté, M. (2021). The authors’ official pytorch sigcgwan implementation.
- Song, J., C. Meng, and S. Ermon (2020). Denoising diffusion implicit models. <https://arxiv.org/abs/2010.02502>.
- Srinivasan, P. and W. J. Knottenbelt (2022). Time-series transformer generative adversarial networks. <https://arxiv.org/abs/2205.11164>.
- Sutskever, I., O. Vinyals, and Q. V. Le (2014). Sequence to sequence learning with neural networks. In Z. Ghahramani, M. Welling, C. Cortes, N. Lawrence, and K. Weinberger (Eds.), *Advances in Neural Information Processing Systems*, Volume 27. Curran Associates, Inc. <https://proceedings.neurips.cc/paper/2014/file/a14ac55a4f27472c5d894ec1c3c743d2-Paper.pdf>.
- van den Berg, T. (2011). Calibrating the ornstein-uhlenbeck (Vasicek) model. <https://www.statisticshowto.com/wp-content/uploads/2016/01/Calibrating-the-Ornstein.pdf>.
- van der Maaten, L. and G. Hinton (2008). Visualizing data using t-sne. *Journal of Machine Learning Research* 9(86), 2579–2605.
- Vasicek, O. (1977). An equilibrium characterization of the term structure. *Journal of Financial Economics* 5(2), 177–188.
- Villani, C. (2008). *Optimal Transport: Old and New*. Grundlehren der mathematischen Wissenschaften. Springer Berlin Heidelberg.
- Yu, Y., A. Srivastava, and S. Canales (2021, feb). Conditional LSTM-GAN for melody generation from lyrics. *ACM Transactions on Multimedia Computing, Communications, and Applications* 17(1), 1–20. <https://doi.org/10.1145%2F3424116>.

A Appendix

A.1 List of githubs for source code

The following list of githubs is used as the source code for several NN models. We made some changes for our specific purpose.

- <https://github.com/FernandoDeMeer/Hierarchical-SigCWGAN>
- <https://github.com/SigCGANs/Conditional-Sig-Wasserstein-GANs>
- <https://github.com/abudesai/timeVAE>
- https://github.com/luphord/nelson_siegel_svensson

Table A1: Model comparison for dataset USDYC1 (Libor curve) (cond=1y)

Rank	Cat	Model	DIST	ACF	BT	Composite
1	NN	CGAN-LSTM	0.995	0.969	0.606	2.570
2	NN	VAE	0.981	0.933	0.674	2.589
3	NN	CWGAN	0.993	0.647	1.573	3.213
4	NN	DIFFUSION	0.899	0.740	1.802	3.441
5	NN	CGAN-FC	0.999	0.724	1.752	3.475

KPI/score: the smaller the value, the better the model. KPIs are calculated for one dataset.
 DIST: distribution score, ACF: autocorrelation score, BT: backtesting score.

Table A2: Number of model parameters for USD Libor dataset (nn1ycond)

Model	GEN/DEC	DIS/ENC	TOTAL	Code Library
CGAN-FC	413,914	665,345	1,079,259	Tensorflow
CWGAN	1,074,138	1,264,385	2,338,523	Torch
DIFFUSION	39,279	0	39,279	GluonTS
CGAN-LSTM	9,929	8,502	18,431	Tensorflow
SIG	182,316	15,220,260	15,402,576	Torch

A.2 Results with 1Y condition for NN models

The results in the Tables [A1](#) and [A2](#) show that with 1-year condition, the NN models have much more parameters but do not have improved model performance.